LETTER

doi:10.1038/nature14665

Reactivation of multipotency by oncogenic PIK3CA induces breast tumour heterogeneity

Alexandra Van Keymeulen[1]*, May Yin Lee[1]*, Marielle Ousset[1], Sylvain Brohée[2], Sandrine Rorive[3,4], Rajshekhar R. Giraddi[1], Aline Wuidart[1], Gaëlle Bouvencourt[1], Christine Dubois[1], Isabelle Salmon[3,4], Christos Sotiriou[2], Wayne A. Phillips[5,6] & Cédric Blanpain[1,7]

Breast cancer is the most frequent cancer in women and consists of heterogeneous types of tumours that are classified into different histological and molecular subtypes[1,2]. *PIK3CA* and *P53* (also known as *TP53*) are the two most frequently mutated genes and are associated with different types of human breast cancers[3]. The cellular origin and the mechanisms leading to *PIK3CA*-induced tumour heterogeneity remain unknown. Here we used a genetic approach in mice to define the cellular origin of *Pik3ca*-derived tumours and the impact of mutations in this gene on tumour heterogeneity. Surprisingly, oncogenic *Pik3ca*^{H1047R} mutant expression at physiological levels[4] in basal cells using keratin (K)5-CreER^{T2} mice induced the formation of luminal oestrogen receptor (ER)-positive/progesterone receptor (PR)-positive tumours, while its expression in luminal cells using K8-CReER^{T2} mice gave rise to luminal ER$^+$PR$^+$ tumours or basal-like ER$^-$PR$^-$ tumours. Concomitant deletion of *p53* and expression of *Pik3ca*^{H1047R} accelerated tumour development and induced more aggressive mammary tumours. Interestingly, expression of *Pik3ca*^{H1047R} in unipotent basal cells gave rise to luminal-like cells, while its expression in unipotent luminal cells gave rise to basal-like cells before progressing into invasive tumours. Transcriptional profiling of cells that underwent cell fate transition upon *Pik3ca*^{H1047R} expression in unipotent progenitors demonstrated a profound oncogene-induced reprogramming of these newly formed cells and identified gene signatures characteristic of the different cell fate switches that occur upon *Pik3ca*^{H1047R} expression in basal and luminal cells, which correlated with the cell of origin, tumour type and different clinical outcomes. Altogether our study identifies the cellular origin of *Pik3ca*-induced tumours and reveals that oncogenic *Pik3ca*^{H1047R} activates a multipotent genetic program in normally lineage-restricted populations at the early stage of tumour initiation, setting the stage for future intratumoural heterogeneity. These results have important implications for our understanding of the mechanisms controlling tumour heterogeneity and the development of new strategies to block *PIK3CA* breast cancer initiation.

Breast cancers can be classified into different histological and molecular subtypes including luminal (ER$^+$ and/or PR$^+$), HER2$^+$ and basal-like/triple-negative (ER$^-$PR$^-$HER2$^-$) cancers, which are usually associated with different gene expression and mutation profiles, prognosis and response to therapies[5]. *PIK3CA* mutations are found in about 30% of breast cancers, more frequently in luminal tumours, although they are also found in basal-like/triple-negative breast cancers[3,6–9]. Expression of oncogenic *Pik3ca*^{H1047R} in all mammary gland lineages using MMTV-Cre mice[4,10–12] or preferentially in luminal progenitors using WAP-Cre mice[13] induces heterogeneous mammary tumours[4,10–13]. The reason for this tumour heterogeneity upon expression of the *Pik3ca*^{H1047R} mutant in the mammary gland is currently unknown.

To determine whether breast tumour heterogeneity is determined by the cancer cell of origin, we developed a genetic strategy allowing the expression of the oncogenic *Pik3ca* mutant at physiological levels using Cre-inducible *Pik3ca*^{H1047R} knock-in mice[4], specifically in basal cells (BCs) using K5-CreER^{T2} or in luminal cells (LCs) using K8-CreER^{T2} mice[14] and followed their fate and tumorigenic potential over time. Tamoxifen (TAM) was administered at a dose that does not impair long-term mammary gland development and homeostasis, and resulted in the specific labelling of about 20% of BCs (Extended Data Fig. 1) in 4–5-week-old K5-CreER^{T2}/*Pik3ca*^{H1047R} mice (Fig. 1a). While it has been suggested that the mammary gland contains bipotent basal stem cells[15,16], our data using K5-CreER^{T2} knock-in or K14-rtTA/TetO-Cre mice, despite the labelling of 20–50% of BCs, showed no contribution of BCs to the luminal lineage (Extended Data Fig. 1). Further lineage-tracing studies that label all BCs or all LCs will be required to determine whether the discrepancy between the different

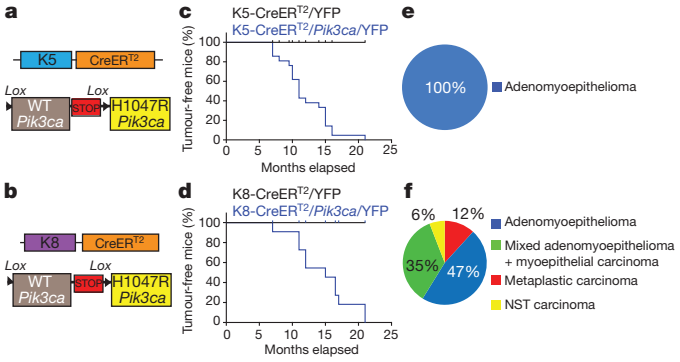

Figure 1 | Oncogenic *Pik3ca* expression in BCs or LCs leads to distinct tumour phenotypes. **a**, **b**, Genetic strategy to target *Pik3ca*^{H1047R} in BCs (**a**) or LCs (**b**). WT, wild type. **c**, **d**, Tumour-free survival curves in K5-CreER^{T2}/*Pik3ca*^{H1047R}/Rosa26-YFP mice ($n = 24$ mice) (latency of 12 ± 4 months (mean ± s.d.)) (**c**) or K8-CreER^{T2}/*Pik3ca*^{H1047R}/Rosa26-YFP mice ($n = 11$ mice) (latency of 15 ± 4 months) (**d**). No tumours were observed in control K5-CreER^{T2}/Rosa26-YFP mice ($n = 10$ mice) (**c**) or in K8-CreER^{T2}/Rosa26-YFP mice ($n = 10$ mice) (**d**). **e**, **f**, Pie chart showing tumour classification in BC-derived (**e**) and LC-derived (**f**) tumours. BC-derived tumours were all classified as adenomyoepitheliomas ($n = 36$ tumours). LC-derived tumours comprised adenomyoepitheliomas ($n = 8$ tumours), mixed adenomyoepithelioma with myoepithelial carcinoma ($n = 6$ tumours), metaplastic carcinoma ($n = 2$ tumours) and invasive carcinoma of NST ($n = 1$ tumour) (**f**). Detailed histological characterization is presented in Extended Data Fig. 2.

[1]Université Libre de Bruxelles, IRIBHM, Brussels B-1070, Belgium. [2]Institut Jules Bordet, Université Libre de Bruxelles, Brussels B-1000, Belgium. [3]Department of Pathology, Erasme Hospital, Université Libre de Bruxelles, Brussels B-1070, Belgium. [4]DIAPATH — Center for Microscopy and Molecular Imaging (CMMI), Gosselies B-6041, Belgium. [5]Surgical Oncology Research Laboratory, Peter MacCallum Cancer Centre, Melbourne 3002, Australia. [6]Sir Peter MacCallum Department of Oncology, University of Melbourne, Parkville 3002, Australia. [7]WELBIO, Université Libre de Bruxelles, Brussels B-1070, Belgium.

*These authors contributed equally to this work.

studies arises from the unspecific and simultaneous labelling of BCs and LCs. BC-derived mammary tumours arose with a latency of about 12 ± 4 months (mean ± standard deviation (s.d.)) and were all luminal-like tumour cells that were ER^+PR^+, surrounded by BCs (Fig. 1c, e and Extended Data Fig. 2a–e), classified by pathologists as adenomyoepithelioma[17] in mouse and humans[17] (Extended Data Fig. 3a–d). Principal component analysis (PCA) and gene clustering analysis of gene expression profile from fluorescence-activated cell sorting (FACS)-isolated tumour cells using the PAM50 gene set showed that these BC-derived-tumours clustered together with the luminal B breast cancer subtype (Extended Data Figs 3 and 4).

The same dose of TAM was administered to 4–5-week-old K8-CreER^{T2}/*Pik3ca*^{H1047R} mice, resulting in the specific labelling of about 20–30% of LCs (Fig. 1b and Extended Data Fig. 1). Mammary tumours arose with a similar latency (15 ± 4 months) (Fig. 1d). Histological and immunofluorescence analysis revealed that these tumours were more heterogeneous, more aggressive and more proliferative than BC-derived tumours. These tumours comprised adenomyoepithelioma, mixed adenomyoepithelioma with myoepithelial carcinoma, invasive carcinoma of no special type (NST), as well as tumours that show features of metaplastic basal-like breast cancers similar to human breast cancers (Fig. 1f and Extended Data Figs 2, 3). Principal component and gene expression clustering analyses from cells isolated from seven different luminal-derived tumours showed that ER^+ tumours clustered together with luminal human breast cancers, NST tumours clustered in between luminal B and $HER2^+$ tumours, and metaplastic carcinoma clustered with basal-like or $HER2^+$ cancers depending on the clustering algorithm (Extended Data Fig. 3j, l), consistent with the phenotypic heterogeneity of the tumours. These results revealed that *Pik3ca*^{H1047R} expression in LCs gives rise to distinct types of tumours that are generally more aggressive compared with BC-derived tumours. The greater tumour heterogeneity found in the LC-derived tumours may arise from the greater plasticity of LCs and/or the heterogeneity of the luminal progenitor populations initially targeted in the K8-CreER^{T2} mice.

We then assessed whether concomitant *p53* deletion affects the phenotype of mammary tumours depending on their cellular origin. K5-CreER^{T2}/*Pik3ca*^{H1047R}/*p53*$^{fl/fl}$ mice treated with TAM rapidly developed skin and other cancers that required terminating the experiment before they developed mammary tumours (data not shown). To circumvent this problem, we used mice heterozygous for *p53* (K5-CreER^{T2}/*Pik3ca*^{H1047R}/*p53*$^{fl/+}$) and another basal Cre driver (K14-rtTA/TetO-Cre/*Pik3ca*^{H1047R}/*p53*$^{fl/+}$) that alleviated the increased early mortality seen with the K5-CreER^{T2}/*Pik3ca*^{H1047R}/*p53*$^{fl/fl}$ mice. BC-derived *p53* heterozygous tumours arose with a latency of 9 ± 2 months and consisted mostly of adenomyoepithelioma luminal-like tumours (42–75%), as well as myoepithelial carcinoma (0–16%), NST tumours (0–12%) and metaplastic carcinoma (12–42%) (Fig. 2 and Extended Data Fig. 5). As previously shown using MMTV-Cre mice[10], *Pik3ca*^{H1047R} expression together with *p53* deletion in LCs dramatically accelerates tumour formation, with a latency of 5 ± 1 months for *p53* homozygous and 9 ± 3 months for *p53* heterozygous mice (Fig. 2). In contrast to BCs, LC-derived p53-deficient tumours always consisted of aggressive carcinomas consisting mostly of metaplastic carcinoma and high-grade myoepithelial carcinoma with characteristics of epithelial-to-mesenchymal transition (Fig. 2 and Extended Data Fig. 5), as previously reported following *Pik3ca*^{H1047R} expression in all mammary gland cells[10,12] and found in human basal-like breast cancers with activation of the PI3K pathway by somatic *PIK3CA* mutations and gene copy number amplification[3,7–9]. Gene expression clustering of these tumours using the PAM50 genes showed that they clustered together with human basal-like or $HER2^+$ subtypes depending on the clustering algorithm (Extended Data Fig. 3k, l). These data demonstrate that concomitant *Pik3ca*^{H1047R} expression and *p53* deletion accelerates tumour development in basal and luminal lineages

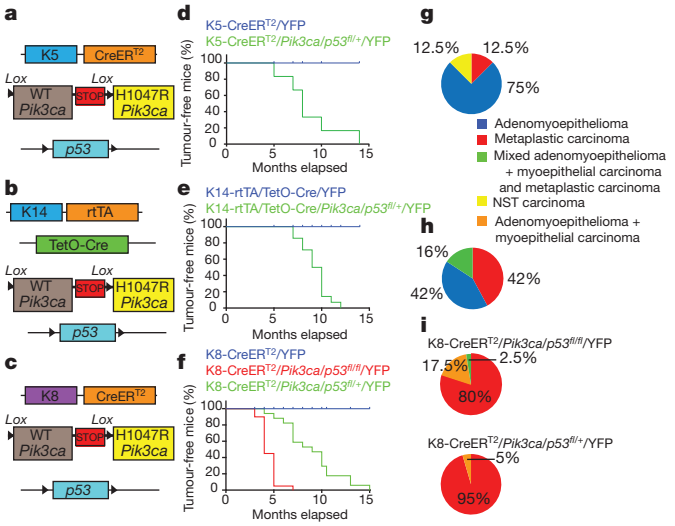

Figure 2 | Oncogenic *Pik3ca* expression and *p53* deletion in BCs or LCs leads more frequently to highly invasive mammary tumours. **a–c**, Genetic strategy to target *Pik3ca*^{H1047R} expression and *p53* deletion in BCs (**a**, **b**) or in LCs (**c**). **d–f**, Tumour-free survival curves in K5-CreER^{T2}/*Pik3ca*^{H1047R}/*p53*$^{fl/+}$/Rosa26-YFP (9 ± 3 months latency; mean ± s.d.) ($n = 6$ mice) (**d**), K14-rtTA/TetO-Cre/*Pik3ca*^{H1047R}/*p53*$^{fl/+}$/Rosa26-YFP (9 ± 1 month latency) ($n = 14$ mice) (**e**), K8-CreER^{T2}/*Pik3ca*^{H1047R}/*p53*$^{fl/fl}$/Rosa26-YFP mice (5 ± 1 month latency) ($n = 20$ mice) and K8-CreER^{T2}/*Pik3ca*^{H1047R}/*p53*$^{fl/+}$/Rosa26-YFP mice (9 ± 3 months latency) ($n = 17$ mice) (**f**). Control mice did not develop tumours ($n = 10$ mice per condition). **g–i**, Pie charts depicting the classification of mammary tumours in K5-CreER^{T2}/*Pik3ca*^{H1047R}/*p53*$^{fl/+}$/Rosa26-YFP ($n = 8$ tumours) (**g**), K14-rtTA/TetO-Cre/*Pik3ca*^{H1047R}/*p53*$^{fl/+}$/Rosa26-YFP ($n = 19$ tumours) (**h**), K8-CreER^{T2}/*Pik3ca*^{H1047R}/*p53*$^{fl/fl}$/Rosa26-YFP ($n = 40$ tumours) and K8-CreER^{T2}/*Pik3ca*^{H1047R}/*p53*$^{fl/+}$/Rosa26-YFP ($n = 22$ tumours) (**i**). Detailed histological characterization is presented in Extended Data Fig. 5.

and that very aggressive metaplastic tumours arise more frequently from oncogenic targeting of LCs than from BCs.

To define further the cellular basis of intratumoural heterogeneity found in *Pik3ca*^{H1047R}-derived tumours, we combined Rosa26-YFP lineage tracing and *Pik3ca*^{H1047R} expression specifically in LCs or BCs and assessed cell fate change over time. Interestingly, as early as 5 weeks after *Pik3ca*^{H1047R} expression in LCs, yellow fluorescent protein (YFP) was also detected in basal-like cells clustered around LCs (Fig. 3a–e and Extended Data Fig. 6), while, as previously described[14], K8-CreER^{T2}-targeted cells consist of a self-sustained unipotent population of LCs (Extended Data Fig. 6a–e). Clonal analysis of LCs expressing oncogenic PIK3CA revealed the presence of bipotent clones containing adjacent LCs and BCs, which were never observed in YFP control LCs (Fig. 3f and Extended Data Fig. 6n–p). The relatively small proportion of $K8^+/K5^+$ BCs compared with $K8^-/K5^+$ BCs suggests that in the initial stage of LC-to-BC transition, these cells expressed markers of both lineages before maturing into basal-like cells and losing expression of LC markers (Fig. 3g and Extended data Fig. 6q–t), which is consistent with the sequential gene expression shown by quantitative polymerase chain reaction with reverse transcription (qRT–PCR) analysis of FACS-isolated BCs and LCs after *Pik3ca*^{H1047R} expression (Extended Data Fig. 6u, v). The proportion of YFP-expressing LCs increased over time, as well as the proportion of YFP^+ BCs (Fig. 3e), suggesting that *Pik3ca*^{H1047R} confers a competitive advantage on luminal targeted cells. To determine functionally whether LCs acquired multipotency upon PIK3CA expression, we tested the ability of *Pik3ca*^{H1047R}-expressing LCs and their BC progeny to reconstitute the mammary gland upon transplantation into mammary fat pads. FACS-isolated LCs expressing *Pik3ca*^{H1047R} were able to form outgrowths of mammary epithelium containing both BCs and LCs (observed in 6 out of 28 transplants), while, as previously

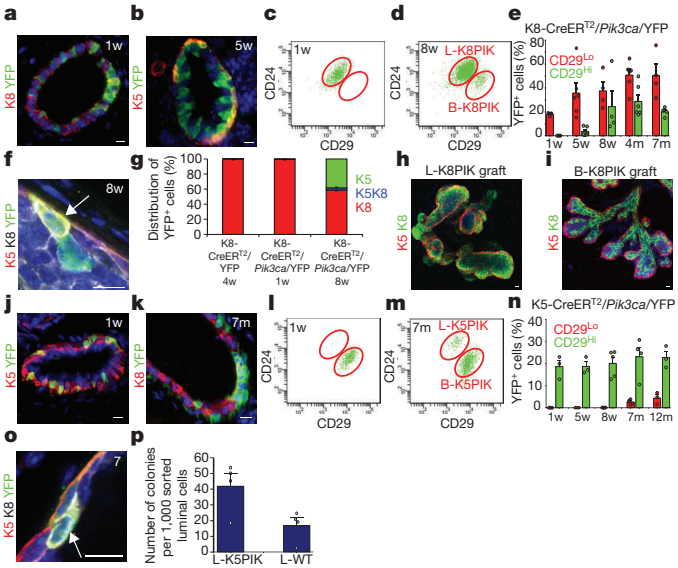

Figure 3 | Oncogenic *Pik3ca* expression induces multipotency in unipotent luminal and basal progenitors. a, b, Immunofluorescence of K8/YFP at 1 week (**a**) and K5/YFP at 5 weeks (**b**) after TAM administration to K8-CreER^{T2}/*Pik3ca*^{H1047R}/Rosa26-YFP mice. m, month; w, week. **c**, **d**, FACS analysis of CD24 and CD29 expression in Lin-YFP$^+$ cells 1 week (**c**) or 8 weeks (**d**) after TAM induction. **e**, Percentage of YFP$^+$ cells within LCs (CD29^{Lo}/CD24$^+$) and BCs (CD29^{Hi}/CD24$^+$) at different time points after TAM administration ($n = 3, 6, 3, 6, 4$ mice for 1 week, 5 weeks, 8 weeks, 4 months and 7 months, respectively). **f**, Immunofluorescence of K8/K5/YFP 8 weeks after clonal induction of K8-CreER^{T2}/*Pik3ca*^{H1047R}/Rosa26-YFP mice. Arrow points to K5/K8/*Pik3ca*^{H1047R}/YFP$^+$ BC newly generated from a LC. **g**, Percentage of YFP$^+$ cells expressing K5 and/or K8 at different time points after *Pik3ca*^{H1047R} expression in LCs ($n = 3$ mice per condition). See Methods for more details. **h**, **i**, Immunofluorescence of K5/K8 of a mammary outgrowth derived from LCs (**h**) or BCs (**i**) from K8-CreER^{T2}/*Pik3ca*^{H1047R}/Rosa26-YFP mice. **j**, **k**, Immunofluorescence of K5/YFP 1 week (**j**) or of K8/YFP 7 months (**k**) after TAM administration to K5-CreER^{T2}/*Pik3ca*^{H1047R}/Rosa26-YFP mice. **l**, **m**, FACS analysis of CD24 and CD29 expression in Lin-YFP$^+$ cells 1 week (**l**) or 7 months (**m**) after TAM induction. **n**, Percentage of YFP$^+$ cells within LCs and BCs at different time points after TAM administration ($n = 3, 3, 5, 4, 3$ mice for 1 week, 5 weeks, 8 weeks, 7 months and 12 months, respectively). **o**, Immunofluorescence for K8/K5/YFP 7 months after clonal *Pik3ca*^{H1047R}/YFP expression in BCs. Arrow points to newly formed K8$^+$YFP$^+$ LC arising from a BC. **p**, Mean number of colonies per 1,000 sorted luminal cells in an *in vitro* colony-forming assay of YFP$^+$ LCs derived from K5-CreER^{T2}/*Pik3ca*^{H1047R}/Rosa26-YFP mice induced for 12 months or wild-type LCs ($n = 3$ biologically independent experiments per condition). Circles, individual data points. Error bars, standard error of the mean (s.e.m.). Scale bars, 10 μm.

described[14,18,19], wild-type LCs derived from K8-CreER^{T2}/Rosa26-YFP mice were not able to form mammary outgrowths in the same conditions (in 0 out of 10 transplants) (Fig. 3h). Likewise, transplantation of newly formed BCs from K8-CreER^{T2}/*Pik3ca*^{H1047R} mice also generated mammary outgrowths containing BCs and LCs (7/11), as efficiently as control BCs (8/10) (Fig. 3i). Altogether these data show that oncogenic *Pik3ca* promotes multilineage differentiation of LCs, inducing cellular heterogeneity at the early stage of the tumour initiation process.

In contrast to the early multilineage differentiation observed after oncogenic PIK3CA expression in LCs, during the first few months after TAM administration to K5-CreER^{T2}/*Pik3ca*^{H1047R}/Rosa26-YFP mice, BCs remained unipotent. Only around 7 months after oncogene expression, newly formed LCs became detectable and progressively increased over time (Fig. 3j–o and Extended Data Fig. 7). Immunostaining and qRT–PCR showed that these newly formed LCs expressed luminal markers at similar levels to wild-type LCs and no longer expressed high levels of basal markers (Extended Data Fig. 7k, l). To determine whether LCs derived from BCs functionally correspond to luminal progenitors, we assessed the clonogenic potential of these cells using a colony-forming assay that only allows the growth of LCs[20]. The number of colonies derived from FACS-isolated LCs after *Pik3ca*^{H1047R} expression in BCs was significantly higher compared with wild-type LCs, supporting the notion that oncogenic PIK3CA promotes the reprogramming of BCs into functional LCs (Fig. 3p). Altogether, these data show that *Pik3ca*^{H1047R} induces multipotency in otherwise lineage-restricted basal and luminal unipotent progenitors, inducing cellular heterogeneity in oncogene-targeted cells before progressing into more invasive tumours.

To define the molecular mechanisms by which *Pik3ca*^{H1047R} promotes multipotency and tumour heterogeneity, we performed transcriptional profiling of FACS-isolated basal-like and luminal-like cells after *Pik3ca*^{H1047R} induction in LCs (K8-CreER^{T2}/*Pik3ca*^{H1047R}/Rosa26-YFP mice) (B-K8PIK and L-K8PIK) and in BCs (K5-CreER^{T2}/*Pik3ca*^{H1047R}/Rosa26-YFP mice) (B-K5PIK and L-K5PIK) (Fig. 3d, m and Supplementary Table 1). Gene expression clustering analysis showed that a profound reprogramming occurred in PIK3CA-(H1047R)-expressing cells as they underwent transition between basal and luminal lineages, becoming molecularly similar to the mammary lineages that they were converted into (Fig. 4a).

To unravel the molecular mechanisms by which oncogenic *Pik3ca* induced changes in cell fate and determine whether these mechanisms are conserved or distinct across different cells of origin, we defined the gene signature induced by the expression of oncogenic *Pik3ca* in each population (that is, B-K5PIK versus B-K5YFP, L-K5PIK versus L-K8YFP, and so on). Only three genes were upregulated in all conditions (*Serpina3n*, *Gdpd3* and *Zfp949*), and most of the genes upregulated by *Pik3ca*^{H1047R} expression were dependent on both the origin of the cell in which *Pik3ca*^{H1047R} was initially expressed and the cell lineage in which the oncogene was currently expressed (Fig. 4b, Supplementary Table 2 and Extended Data Fig. 8). While *Pik3ca*^{H1047R} induced the expression of specific genes according to their cellular origin and their basal or luminal phenotypes, 51 annotated genes were commonly upregulated in L-K5PIK and in B-K8PIK, including the long non-coding RNA *Neat1* and the transcription factor *Runx2*, which both regulate mammary cell fate[21,22], genes regulating signal transduction (for example, *Sfrp2*), cellular metabolism (for example, *Tktl1*, *Bdh1*) and cell adhesion (for example, *EphB2*, *Trio*) (Fig. 4b, c and Supplementary Table 2), suggesting that common and distinct mechanisms induce cell fate changes upon oncogenic *Pik3ca* expression.

BC-to-LC fate transition induced by oncogenic *Pik3ca* induced the expression of a distinct set of genes (basal-to-luminal multipotent signature) (Fig. 4). Some of these genes, such as *Ntrk3* (also known as *TrkC*), were already upregulated in BCs after *Pik3ca*^{H1047R} expression (Supplementary Table 2), suggesting that they represent the signature of their BC of origin. After BC-to LC fate transition, *Pik3ca*^{H1047R} expression induced genes that are specific for the newly formed LCs, including *Nrtk2* (also known as *TrkB*), a neurotrophin receptor expressed in wild-type BCs and transiently expressed in LCs during *Pik3ca*^{H1047R}-induced BC-to-LC fate transition (Fig. 4d and Extended Data Fig. 7m). NRTK2 and NRTK3 have previously been shown to be expressed in breast cancers and regulate survival of breast cancer stem cells in response to chemotherapy[23,24]. In addition, a translocation leading to a gene fusion between *Etv6* and *Ntrk3* causes breast tumours in both mouse and humans[25,26]. *Etv6-Ntrk3* expression in the mammary gland predominantly induces the same type of bipotent mammary tumours[26] that arise from *Pik3ca*^{H1047R} expression in BCs, supporting a role for the *Pik3ca*/*Ntrk2*–*Ntrk3* axis in the establishment of bipotency during breast tumour initiation. The basal-to-luminal upregulated multipotent signature also contained genes commonly upregulated in L-K8PIK (Extended Data Fig. 8k), reflecting the consequence of PIK3CA expression in LCs.

In contrast, the luminal-to-basal multipotent signature was characteristic of a wounding and proliferation response marked by the upregulation of *Il33* (also known as alarmin; a cytokine that has been shown to be overexpressed in breast cancers and attenuates NK response against tumour cells[27,28]), *Il24a*, *Krt16*, *Itgb6*, *Itga2*, *Itga5*, *Tnc*, *Cd109*, *Plau*, *Wnt10a*, *Timp3*, *Inhba*, *Ngf*, *Ereg*, *Ccdn1* and *Ccdn2* (Fig. 4e). As found during BC-to-LC transition, most of the luminal-to-basal multipotent signature genes were specific for the newly formed BCs (for example, *Ereg*, *Ccnd1*, *Wnt10a*, *Il33*); a significant fraction of these genes (for example, *Krt16*, *Il24a*, *Ccnd2*, *Inhba*, *Tnc*) were already upregulated in LCs targeted by oncogenic PIK3CA, suggesting that they represent the signature of the LC of origin (Supplementary Tables 2, 3 and Extended Data Fig. 8).

To define the relevance of these multipotency gene signatures to tumour progression, we assessed the expression of these genes in *Pik3ca*^{H1047R}-derived tumours. Some luminal-to-basal multipotent signature genes such as *Il24a*, *Krt16* and *Plau* were only upregulated during the initial stage of reprogramming and downregulated thereafter, while other genes such as *Col11a1*, the epidermal growth factor rector (EGFR) ligand *Ereg*, *Inhba*, *Wnt10a* and *Tnc* continued to be expressed, or even further increased, in basal-like breast cancers arising from LCs (Fig. 4e, f). Similarly, *Ntrk2* and *Ntrk3* were expressed or even further upregulated in K5-CreER^{T2}/*Pik3ca*^{H1047R}-derived luminal tumours (Fig. 4f). These data indicate that some of the genes associated with cell fate transition during the early steps of tumour initiation increase with tumour progression.

To define the relevance of the *Pik3ca*^{H1047R}-induced multipotent gene signatures in human breast cancers, we assessed whether the different multipotent signatures correlated with a particular molecular breast cancer subtype[29] or disease-free survival in a cohort of systemically untreated breast cancer patients[30]. Interestingly, the luminal-to-basal transition gene signature was strongly associated with basal-like breast cancers (Fig. 4g). Higher expression levels of this gene signature or individual genes such as *NGF*, *INHBA*, *ITGB6* and *WNT10A* were associated with poor clinical outcome (Fig. 4h and Extended data Fig. 9), consistent with the more aggressive tumour types induced by *Pik3ca*^{H1047R} expression in LCs. In contrast, the BC-to-LC fate signature was associated with luminal A and normal-like human breast cancers (Fig. 4i). High gene expression levels of this gene signature were significantly associated with better prognosis (Fig. 4j), consistent with the less aggressive tumours arising from BCs. These data indicate that the genetic program associated with *Pik3ca*^{H1047R}-induced multipotency correlated with distinct molecular subtypes of human breast cancers and their levels of expression correlated with distinct clinical outcome.

Our study shows that the cell of origin controls tumour heterogeneity in *Pik3ca*^{H1047R}-induced mammary tumours. *Pik3ca*^{H1047R} expression in LCs gives rise to aggressive basal-like tumours while expression in BCs gives rise to less aggressive luminal-like tumours. We demonstrate that *Pik3ca*^{H1047R} induced multipotency in unipotent progenitors. The promotion of multipotency induced by *Pik3ca*^{H1047R} is regulated by common and cell-lineage-specific molecular mechanisms that are influenced by the cellular origin in which the oncogene is initially expressed, setting the stage for future tumour heterogeneity and influencing clinical outcome in patients with breast cancers.

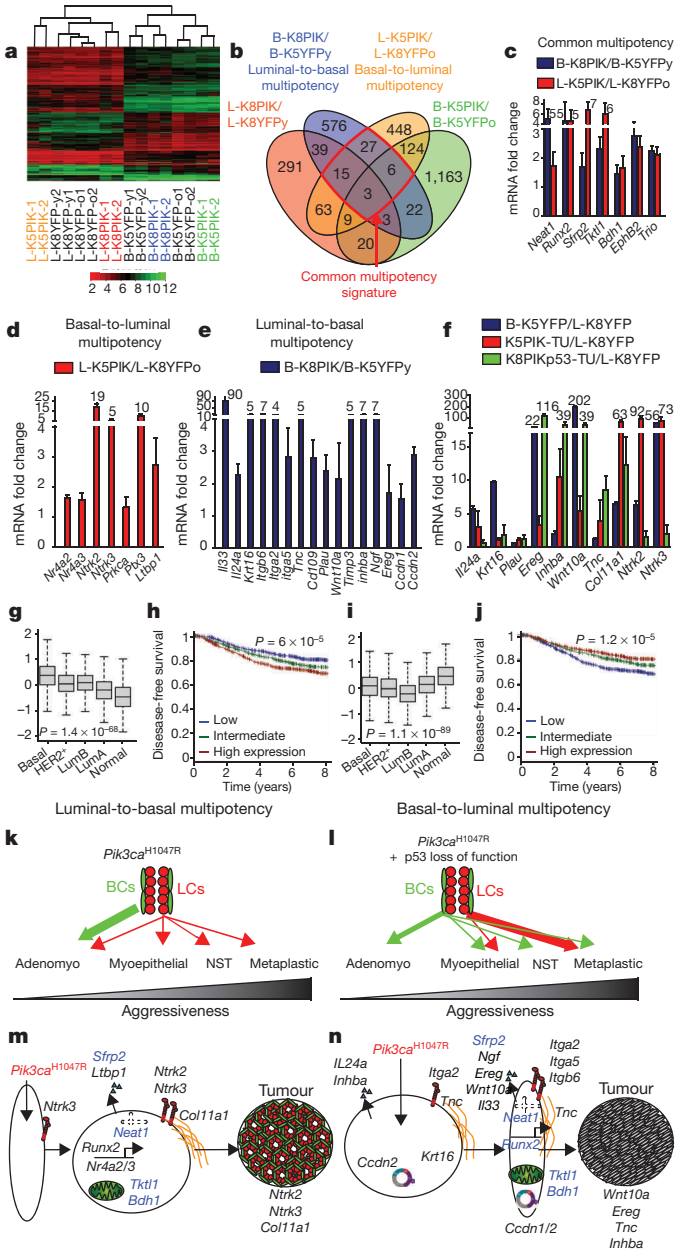

Figure 4 | Molecular characterization of oncogenic *Pik3ca*-induced multipotency. **a**, Hierarchical gene expression clustering of BCs and LCs with or without *Pik3ca*^{H1047R} expression. Green and red correspond to high and low expressed genes, respectively. The two major branches of the tree are supported by bootstrap values of 100. o, induced for 10–12 months; y, induced for 8 weeks. **b**, Venn diagram of upregulated genes (>1.5 fold) after *Pik3ca*^{H1047R} expression in BCs and LCs. **c**–**e**, qRT–PCR analysis of genes belonging to the common (**c**), basal-to-luminal (**d**), or luminal-to-basal multipotency signature (**e**) in B-K8PIK and L-K5PIK cell population, 8 weeks and 10–12 months after *Pik3ca*^{H1047R} expression, respectively, compared with their age-matched controls. Gene expression was normalized to *Gapdh* housekeeping gene ($n = 4$ biologically independent samples). **f**, qRT–PCR analysis of the multipotency signature genes in control cells, in BC-derived adenomyoepithelioma and in LC-derived metaplastic tumours. Data were normalized to gene expression in age-matched control LCs (L-K8YFPo) ($n = 4$ biologically independent samples). **g**, **i**, Expression levels of the luminal-to-basal (**g**) or basal-to-luminal (**i**) multipotency signature in a large set of breast cancer patients according to their PAM50 subtype. Lum, luminal. **h**, **j**, Disease-free survival in untreated patients according to the level of expression of the genes of the luminal-to-basal (**h**) or basal-to-luminal (**j**) multipotency signature. **k**–**n**, Summary of the role of the cancer cell of origin in regulating *Pik3ca*^{H1047R}-induced tumour heterogeneity. **k**, Expression of *Pik3ca*^{H1047R} in BCs gives rise to luminal-like tumours, while in LCs *Pik3ca*^{H1047R} gives rise to more heterogeneous and aggressive tumours. Types of carcinoma are noted at the bottom of the panel. Adenomyo, adenomyoepithelioma. **l**, Additional *p53* deletion promotes *Pik3ca*^{H1047R}-induced tumour heterogeneity in BCs and leads to more aggressive metaplastic carcinoma in LCs. **m**, **n**, Model of *Pik3ca*^{H1047R}-induced multipotency in LCs and BCs. Genes shown are upregulated during cell fate change. Genes highlighted in blue belong to the common multipotency signature. Error bars, s.e.m.

Online Content Methods, along with any additional Extended Data display items and Source Data, are available in the online version of the paper; references unique to these sections appear only in the online paper.

Received 30 July 2014; accepted 15 June 2015.
Published online XX 2015.

1. Weigelt, B., Geyer, F. C. & Reis-Filho, J. S. Histological types of breast cancer: how special are they? *Mol. Oncol.* **4,** 192–208 (2010).
2. Perou, C. M. *et al.* Molecular portraits of human breast tumours. *Nature* **406,** 747–752 (2000).
3. Network, C. G. A. Comprehensive molecular portraits of human breast tumours. *Nature* **490,** 61–70 (2012).
4. Tikoo, A. *et al.* Physiological levels of *Pik3ca*^{H1047R} mutation in the mouse mammary gland results in ductal hyperplasia and formation of ERα-positive tumors. *PLoS ONE* **7,** e36924 (2012).
5. Prat, A., Ellis, M. J. & Perou, C. M. Practical implications of gene-expression-based assays for breast oncologists. *Nature Rev. Clin. Oncol.* **9,** 48–57 (2012).
6. Shah, S. P. *et al.* The clonal and mutational evolution spectrum of primary triple-negative breast cancers. *Nature* **486,** 395–399 (2012).
7. Stemke-Hale, K. *et al.* An integrative genomic and proteomic analysis of PIK3CA, PTEN, and AKT mutations in breast cancer. *Cancer Res.* **68,** 6084–6091 (2008).
8. López-Knowles, E. *et al.* PI3K pathway activation in breast cancer is associated with the basal-like phenotype and cancer-specific mortality. *Int. J. Cancer* **126,** 1121–1131 (2010).
9. Tilch, E. *et al.* Mutations in EGFR, BRAF and RAS are rare in triple-negative and basal-like breast cancers from Caucasian women. *Breast Cancer Res. Treat.* **143,** 385–392 (2014).
10. Adams, J. R. *et al.* Cooperation between Pik3ca and p53 mutations in mouse mammary tumor formation. *Cancer Res.* **71,** 2706–2717 (2011).
11. Liu, P. *et al.* Oncogenic PIK3CA-driven mammary tumors frequently recur via PI3K pathway-dependent and PI3K pathway-independent mechanisms. *Nature Med.* **17,** 1116–1120 (2011).
12. Yuan, W. *et al.* Conditional activation of *Pik3ca*^{H1047R} in a knock-in mouse model promotes mammary tumorigenesis and emergence of mutations. *Oncogene* **32,** 318–326 (2013).
13. Meyer, D. S. *et al.* Luminal expression of PIK3CA mutant H1047R in the mammary gland induces heterogeneous tumors. *Cancer Res.* **71,** 4344–4351 (2011).
14. Van Keymeulen, A. *et al.* Distinct stem cells contribute to mammary gland development and maintenance. *Nature* **479,** 189–193 (2011).
15. Rios, A. C., Fu, N. Y., Lindeman, G. J. & Visvader, J. E. *In situ* identification of bipotent stem cells in the mammary gland. *Nature* **506,** 322–327 (2014).
16. Wang, D. *et al.* Identification of multipotent mammary stem cells by protein C receptor expression. *Nature* **517,** 81–84 (2015).
17. Hayes, M. M. Adenomyoepithelioma of the breast: a review stressing its propensity for malignant transformation. *J. Clin. Pathol.* **64,** 477–484 (2011).
18. Shackleton, M. *et al.* Generation of a functional mammary gland from a single stem cell. *Nature* **439,** 84–88 (2006).
19. Stingl, J. *et al.* Purification and unique properties of mammary epithelial stem cells. *Nature* **439,** 993–997 (2006).
20. Shehata, M. *et al.* Phenotypic and functional characterisation of the luminal cell hierarchy of the mammary gland. *Breast Cancer Res.* **14,** R134 (2012).
21. Standaert, L. *et al.* The long noncoding RNA Neat1 is required for mammary gland development and lactation. *RNA* **20,** 1844–1849 (2014).
22. Owens, T. W. *et al.* Runx2 is a novel regulator of mammary epithelial cell fate in development and breast cancer. *Cancer Res.* **74,** 5277–5286 (2014).
23. Jin, W. *et al.* TrkC plays an essential role in breast tumor growth and metastasis. *Carcinogenesis* **31,** 1939–1947 (2010).
24. Yin, B. *et al.* The TrkB^{+} cancer stem cells contribute to post-chemotherapy recurrence of triple-negative breast cancers in an orthotopic mouse model. *Oncogene* **34,** 761–770 (2015).
25. Euhus, D. M., Timmons, C. F. & Tomlinson, G. E. *ETV6-NTRK3*—Trk-ing the primary event in human secretory breast cancer. *Cancer Cell* **2,** 347–348 (2002).
26. Li, Z. *et al. ETV6-NTRK3* fusion oncogene initiates breast cancer from committed mammary progenitors via activation of AP1 complex. *Cancer Cell* **12,** 542–558 (2007).
27. Milovanovic, M. *et al.* IL-33/ST2 axis in inflammation and immunopathology. *Immunol. Res.* **52,** 89–99 (2012).
28. Wu, J. *et al.* Identification and functional analysis of 9p24 amplified genes in human breast cancer. *Oncogene* **31,** 333–341 (2012).
29. Parker, J. S. *et al.* Supervised risk predictor of breast cancer based on intrinsic subtypes. *J. Clin. Oncol.* **27,** 1160–1167 (2009).
30. Haibe-Kains, B. *et al.* A three-gene model to robustly identify breast cancer molecular subtypes. *J. Natl. Cancer Inst.* **104,** 311–325 (2012).

Supplementary Information is available in the online version of the paper.

Acknowledgements C.B. is an investigator of WELBIO, A.V.K. is Chercheur Qualifié of the FNRS, C.S. is Maître de Recherche of the FNRS, M.Y.L. is supported by the Agency for Science, Technology and Research (A*STAR, Singapore) fellowship, M.O. and A.W. are supported by FNRS fellowships, R.R.G. is supported by a TELEVIE fellowship and S.B. is supported by the foundation ''Amis de l'institut Jules Bordet''. The Center for Microscopy and Molecular Imaging is supported by the European Regional Development Fund and Wallonia. W.A.P. is supported by project grants from the National Health and Medical Research Council of Australia. This work was supported by the FNRS, TELEVIE, a research grant from the Fondation Contre le Cancer, the ULB fondation, the Fond Yvonne Boël, the Fond Gaston Ithier, the foundation Bettencourt Schueller, the foundation Baillet Latour, and the European Research Council.

Author Contributions C.B. and A.V.K. designed the experiments and performed data analysis. A.V.K., M.Y.L. and M.O. performed all the experiments. S.B. and C.S. performed the bioinformatic analysis of gene expression and comparison with human breast cancer expression and gene amplification on human samples. S.R. and I.S. helped to perform the histological classification of mouse mammary tumours with regard to their similarities with human breast cancers. G.B. provided technical support. C.D. provided technical support for cell sorting. A.W. and R.R.G. helped with some experiments. W.A.P. provided animals and critically reviewed the manuscript. C.B. and A.V.K. wrote the manuscript.

Author Information Microarrays have been deposited in the Gene Expression Omnibus under accession number GSE69290. Reprints and permissions information is available at www.nature.com/reprints. The authors declare no competing financial interests. Readers are welcome to comment on the online version of the paper. Correspondence and requests for materials should be addressed to C.B. (Cedric.Blanpain@ulb.ac.be) or A.V.K. (avkeymeu@ulb.ac.be).

METHODS

Mice. Rosa26-YFP mice[31] were obtained from the Jackson laboratory. K5-CreER^{T2}, and K8-CreER^{T2} mice were described previously[14]. K14-rtTA mice[32] were provided by E. Fuchs. TetO-Cre mice[33] were provided by A. Nagy. *Pik3ca*^{H1047R} knock-in mice, in which wild-type exon 20 is replaced by H1047R mutant exon 20 upon Cre recombination, were described previously[4]. *p53*$^{fl/fl}$ mice[34] were obtained from the National Cancer Institute at Frederick.

All experimental mice used in this study were female, mixed strains and more than 6 weeks old. No statistical methods were used to predetermine sample size. For all experiments presented in this study, the sample size was large enough to measure the effect size. The experiments were not randomized. The investigators were not blinded to allocation during experiments and outcome assessment. Mice designated within the tumour cohort were killed when a palpable mass of maximum 1 cm^3 was detected. Mouse colonies were maintained in a certified animal facility in accordance with European guidelines. Ethical protocol was approved by the local ethical committee for animal welfare (CEBEA) from the Université Libre de Bruxelles (protocols 363 and 527).

Targeting expression of YFP and/or PIK3CA(H1047R) and deletion of p53. Four- to five-week-old K5-CreER^{T2}/*Pik3ca*^{H1047R}/Rosa26-YFP, K8-CreER^{T2}/*Pik3ca*^{H1047R}/Rosa26-YFP, K8-CreER^{T2}/*Pik3ca*^{H1047R}/*p53*$^{fl/fl}$/Rosa26-YFP, K8-CreER^{T2}/*Pik3ca*^{H1047R}/*p53*$^{fl/+}$/Rosa26-YFP, K5-CreER^{T2}/*Pik3ca*^{H1047R}/*p53*$^{fl/+}$/Rosa26-YFP, K5-CreER^{T2}/Rosa26-YFP and K8-CreER^{T2}/Rosa26-YFP mice were induced with 15 mg of tamoxifen (TAM) (Sigma; diluted in sunflower seed oil, Sigma) by intraperitoneal injection (3 injections of 5 mg every 3 days). TAM administration induced a transient delay in mammary gland development during puberty but there was no long-term effect on mammary gland development and homeostasis[35]. Five-week-old K14-rtTA/TetO-Cre/*Pik3ca*^{H1047R}/*p53*$^{fl/+}$/Rosa26-YFP and K14-rtTA/TetO-Cre/Rosa26-YFP mice were induced by oral administration of doxycycline food diet (1 g kg^{-1}; BIO-SERV) for 5 days. For clonal analyses, 4-to-5-week-old K8-CreER^{T2}/*Pik3ca*^{H1047R}/Rosa26-YFP and K5-CreER^{T2}/*Pik3ca*^{H1047R}/Rosa26-YFP mice were respectively induced with 0.05 mg or 2 mg TAM by intraperitoneal injection. For induction in adult mice, 8-week-old K8-CreER^{T2}/*Pik3ca*^{H1047R}/Rosa26-YFP mice were induced with 15 mg of TAM by intraperitoneal injection (3 injections of 5 mg every 3 days).

Histology and immunostaining on sections. For immunofluorescence, dissected inguinal mammary glands or tumour samples were pre-fixed for 2 h in 4% paraformaldehyde at room temperature. Tissues were washed three times with PBS for 5 min and incubated overnight in 30% sucrose in PBS at 4 °C. Tissues were embedded in OCT and kept at −80 °C. Sections of 5 µm were cut using a HM560 Microm cryostat (Mikron Instruments).

For immunofluorescence, tissue sections were incubated in blocking buffer (5% horse serum, 1% BSA, 0.2% Triton-X in PBS) for 1 h at room temperature. The different primary antibodies combinations were incubated overnight at 4 °C. Sections were then rinsed three times for 5 min in PBS and incubated with corresponding secondary antibodies diluted at 1:400 in blocking buffer for 1 h at room temperature. The following primary antibodies were used: anti-GFP (rabbit, 1:1,000, A11122, Molecular Probes), anti-GFP (chicken, 1:1,000, ab13970, Abcam), anti-K8 (rat, 1:1000, Troma-I, Developmental Studies Hybridoma Bank, University of Iowa), anti-K14 (rabbit, 1:1,000, PRB-155P-0100, Covance), anti-K14 (chicken, 1:1,000, SIG-3476-0100, Covance), anti-K5 (rabbit, 1:1,000, PRB-160P-0100, Covance), anti-K19 (rat, 1:500, Troma-III, Developmental Studies Hybridoma Bank, University of Iowa), anti-ER (rabbit, 1:300, sc-542, Santa Cruz), anti-PR (rabbit, 1:300, sc-7208, Santa Cruz), anti-Her2 (rabbit, 1:300, 2165, Cell Signaling), anti-Ki67 (rabbit, 1:500, ab15580, abcam), anti-E-cadherin (rat, 1:1,000, 14-3249-82, eBioscience), anti-vimentin (rabbit, 1:400, ab92547, Abcam), anti-Nrtk2 (rabbit, 1:500, sc-12, Santa Cruz), anti-p63 (rabbit, 1:100, Mab306-05, Santa Cruz), anti-SMA-Cy3 (mouse, 1:500, C6198, Sigma-Aldrich), anti-claudin 3 (rabbit, 1:300, 34-1700, Invitrogen). The following secondary antibodies were used: anti-rabbit, anti-rat, anti-chicken conjugated to AlexaFluor488 (Molecular Probes), to Rhodamine Red-X or to Cy5 (JacksonImmunoResearch). Nuclei were stained with Hoechst solution (1:2,000) and slides were mounted in DAKO mounting medium supplemented with 2.5% Dabco (Sigma).

For paraffin-embedded tissues, dissected mammary glands were pre-fixed overnight, 4 °C in paraformaldehyde 4%. Tissues were washed three times with PBS. Prior to automated paraffin processing, tissues were washed in tap water and kept in isopropanol 70%. Five-micrometre sections were made with a Leica RM2245 microtome.

Haematoxylin and eosin staining was performed as previously described[36]. p63 staining on tumour paraffin sections were performed on an automated IHC platform (Ventana Discovery XT). Briefly, paraffin sections were deparaffinized and rehydrated. The antigen unmasking procedure was performed for 36 min at 95 °C in EDTA (pH 9). Slides were incubated with the anti-p63 (clone 7JUL, 1:100, Leica) for 3 h, followed by a linker rabbit anti-mouse (clone M1gG51-4, abcam 1:750) for 16 min. Finally, slides were incubated with the OmniMap HRP-conjugated anti-rabbit antibody (Ventana) for 12 min. Standard ABC kit, and ImmPACT DAB (Vector Laboratories) were used for the detection of HRP activity. Nuclei staining was done with Mayer's Hematoxylin (Labonord), followed by dehydration and mounting with SafeMount (Labonord).

Whole-mount mammary gland immunofluorescence. For clonal analyses, dissected inguinal mammary glands were incubated in 2 ml HBSS plus 30 U ml^{-1} collagenase plus 300 µg ml^{-1} hyaluronidase (Sigma) for 30 min at 37 °C under agitation. After three washes of 5 min with HBSS, mammary glands were fixed in 4% paraformaldehyde for 2 h at room temperature, washed three times for 10 min in PBS under agitation and incubated in blocking buffer (5% horse serum, 1% BSA, 0.8% Triton-X in PBS) for 3 h at room temperature. The primary antibody combination, diluted in the blocking buffer, was incubated overnight at room temperature under agitation. Samples were washed three times for 10 min in PBS/0.2% Tween-20 and incubated in secondary antibodies diluted in the blocking buffer for 5 h under agitation. Cell nuclei were stained with Hoechst for 30 min (1:1,000 in PBS/0.2% Tween-20). Samples were mounted on slides in DAKO mounting medium supplemented with 2.5% Dabco (Sigma).

Staining on human breast cancer sections. Tissue samples were obtained retrospectively from archival formalin-fixed and paraffin-embedded samples in the Department of Pathology of the Erasme Hospital. Histopathological diagnoses were reviewed and assessed according to the 2012 World Health Organization Classification. Sections of 5 µm were subjected to standard immunochemistry (IHC) as previously described[36] using respectively monoclonal anti-CK8/18 (1:200; clone 5D3; BioGenex), anti-CK14 (1:100; clone LL002; Leica) and anti-P63 (1:200; clone 7JUL; Leica) antibodies. Staining was visualized with streptavidin-biotin-peroxydase complex kit reagents (BioGenex) using diaminobenzidine/H_2O_2 as the chromogenic substrate. Counterstaining with haematoxylin concluded the processing. Nuclei staining was done with Mayer's Haematoxylin (Labonord), followed by dehydration and mounting with SafeMount (Labornord).

Microscope image acquisition. Pictures were acquired on an Axio Observer Z1 Microscope using ×10 and ×40 Zeiss EC Plan-NEOFLUAR objectives, with an AxioCamMR3 camera and using the Axiovision software (Carl Zeiss). Confocal images in Fig. 3f, h, i, o and Extended Data Fig. 6f, h–l, n, o, q–t and Extended Data Fig. 7i, m, were acquired at room temperature using a Zeiss LSM780 multiphoton confocal microscope fitted on an Axiovert M200 inverted microscope equipped with C-Apochromat (×40 = 1.2 numerical aperture) water immersion objectives (Carl Zeiss). Optical sections of 1,024 × 1,024 pixels, were collected sequentially for each fluorochrome. The data sets generated were merged and displayed with the ZEN software.

Mammary gland and tumour cell dissociation. Mammary glands were dissected and lymph nodes removed. Tissues were briefly washed in HBSS, and chopped with a McIwain tissue chopper. Chopped tissues were placed in HBSS plus 300 U ml^{-1} collagenase (Sigma) plus 300 µg ml^{-1} hyaluronidase (Sigma) and digested for 2 h at 37 °C under agitation. Physical dissociation using a P1000 pipette was done every 15 min throughout the enzymatic digestion duration. EDTA at a final concentration of 5 mM was added for 10 min to the resultant organoid suspension, followed by 0.25% Trypsin-EGTA for 2 min (only in the case of normal mammary glands) before filtration through a 70 µm mesh, two successive washes in 2% FBS/PBS and antibody labelling.

Cell labelling, flow cytometry and sorting. Two-to-five million cells per condition were incubated in 250 µl 2% FBS/PBS with flurochrome-conjugated primary antibodies for 30 min, vortexing every 10 min. Cells were washed with 2% FBS/PBS and were resuspended in 2.5 µg ml^{-1} 4′,6-diamidino-2-phenylindole (DAPI; Invitrogen) before analysis. Primary antibodies used were: PE-Cy7-conjugated anti-CD24 (1:50, clone M1/69, BD Biosciences), APC-conjugated anti-CD29 (1:50, clone eBioHMb1-1, eBiosciences), PE-conjugated anti-CD45 (1:50, clone 30-F11, eBiosciences), PE-conjugated anti-CD31 (1:50, clone MEC 13.33, BD Biosciences), PE-conjugated anti-CD140a (1:50, clone APA5, eBiosciences). Data analysis and cell sorting were performed on a FACSAria sorter using the FACS DiVa software (BD Biosciences). Dead cells were excluded with DAPI; CD45-, CD31- and CD140a-positive cells were excluded (Lin$^-$) before analysis of the YFP$^+$ cells. For profile analysis, a minimum of 1,000 YFP$^+$ cells were analysed per sample.

Tumour harvesting and classification. Tumours were detected by mammary gland palpation. Mice were killed when one tumour reached a maximum of 1 cm diameter. The K5-CreER^{T2}/*Pik3ca*^{H1047R}/Rosa26-YFP mice presented 1 tumour in 58%, 2 tumours in 25%, and 3 or more tumours in 17% of the cases at the time of analysis (a total of 36 tumours from 24 mice were analysed). The K8-CreER^{T2}/*Pik3ca*^{H1047R}/Rosa26-YFP mice presented 1 tumour in 64%, 2 tumours in 18%, and 3 or more tumours in 18% of the cases at the time of analysis (a total of 17 tumours from 11 mice were analysed). The K5-CreER^{T2}/*Pik3ca*^{H1047R}/*p53*$^{fl/+}$/Rosa26-YFP mice presented 1 tumour in 83%, and 3 tumours in 17% of the cases

at the time of analysis (a total of 8 tumours from 6 mice were analysed). The K14-rtTA/TetO-Cre/*Pik3ca*^{H1047R}/*p53*$^{fl/+}$/Rosa26-YFP mice presented 1 tumour in 57%, 2 tumours in 36%, and 3 or more tumours in 7% of the cases at the time of analysis (a total of 19 tumours from 14 mice were analysed). The K8-CreER^{T2}/*Pik3ca*^{H1047R}/*p53*$^{fl/fl}$/Rosa26-YFP mice presented 1 tumour in 20%, 2 tumours in 45%, and 3 or more tumours in 35% of the cases at the time of analysis (a total of 40 tumours from 20 mice were analysed). The K8-CreER^{T2}/*Pik3ca*^{H1047R}/*p53*$^{fl/+}$/Rosa26-YFP mice presented 1 tumour in 71%, and 2 tumours in 29% of the cases at the time of analysis (a total of 22 tumours from 17 mice were analysed). For each harvested tumour, the tumour was cut in three pieces, one for paraffin embedding, one for OCT embedding, and one for cell sorting and RNA extraction. Tumour classification was done based on histological features.

Mammary colony-forming assay. Luminal YFP$^+$ cells from K5-CreER^{T2}/*Pik3ca*^{H1047R}/Rosa26-YFP mice induced for 12 months were flow-sorted as a single-cell suspension based on their Lin$^-$ CD29^{Lo}CD24$^+$YFP$^+$ profile. Control YFP$^-$ luminal cells from K5-CreER^{T2}/Rosa26-YFP induced for 12 months were sorted based on their CD29^{Lo}CD24$^+$ profile. Luminal cells were cultured with irradiated NIH 3T3 feeder cells in Mouse-Epicult B media (Stem Cell Technologies) supplemented with 10 ng ml^{-1} epidermal growth factor (Sigma-Aldrich), 10 ng ml^{-1} basic fibroblast growth factor (R&D Systems), 4 μg ml^{-1} heparin (Sigma-Aldrich), 1 mg ml^{-1} bovine serum albumin (BSA; Sigma-Aldrich), 5% FBS (Life Technologies), 50 units ml^{-1} penicillin and 50 μg ml^{-1} streptomycin (Life Technologies), as previously described[20]. After 1 week, colonies were fixed with methanol, stained with Giemsa stain (Sigma-Aldrich) and counted manually.

Mammary fat pad transplantation and analysis. Eight thousand LCs from K8-CreER^{T2}/*Pik3ca*^{H1047R}/Rosa26-YFP or control K8-CreER^{T2}/Rosa26-YFP or 1,350 BCs from K8-CreER^{T2}/*Pik3ca*^{H1047R}/Rosa26-YFP or control K14-rtTA/TetO-Cre/Rosa26-YFP induced for 4 months were sorted based on their Lin$^-$YFP$^+$CD29^{Lo}CD24$^+$ or Lin$^-$YFP$^+$CD29^{Hi}CD24$^+$ profiles. LCs were resuspended in 10 μl DMEM plus 50% bovine serum. BCs were sorted in the presence of 10 μM of Rock inhibitor (Y27632, Sigma) and resuspended in 75% DMEM/25% matrigel. Cell suspension was injected into the fourth mammary gland of 3-to-4-week-old NOD-SCID mice that had been cleared of endogeneous epithelium as previously described[18,19]. Recipient mice were mated 4 weeks after the transplantation, and killed 2-to-3 weeks later, when fully pregnant. Recipient glands were dissected and stained for GFP, K8 and K5 as whole mounts. An outgrowth was defined as an epithelial structure comprising ducts and lobules and/or terminal end buds.

Quantification of keratin$^+$ cells within YFP$^+$ cells. A total of 1,907, 1,704 and 2,391 YFP$^+$ cells from three different mice per condition were analysed respectively in K8-CreER^{T2}/Rosa26-YFP induced 4 weeks, K8-CreER^{T2}/*Pik3ca*^{H1047R}/Rosa26-YFP induced 1 week and 8 weeks on 5 μm cryosections stained for K5, K8 and GFP. Coexpression of these markers was analysed with a confocal microscope. Cells were scored as K8$^+$K5$^-$ (K8), K8$^+$K5$^+$ (K5K8) or K8$^-$K5$^+$ (K5) and are shown in Fig. 3g.

Quantification of clone composition. Mammary glands were processed as whole mount and stained for K8, K5 and GFP. Clones were analysed by confocal microscopy. A total of 822, 936, 714 and 360 clones from three independent mice per condition were analysed in K8-CreER^{T2}/*Pik3ca*^{H1047R}/Rosa26-YFP induced for 1 week, induced for 10 weeks, and in K5-CreER^{T2}/*Pik3ca*^{H1047R}/Rosa26-YFP induced for 1 week and induced for 7 months respectively at dose of TAM that labelled very few and isolated cells. The clones were scored in three classes according to their keratin expression: luminal clones, composed only of K8$^+$ cells, basal clones, composed only of K5$^+$ cells, and mixed clones, composed of K8$^+$ and K5$^+$ cells. These data are shown in Extended Data Fig. 6p and Extended Data Fig. 7j.

Quantification of percentage YFP-labelled cells. The percentage of YFP labelled cells within the luminal and basal populations was quantified by FACS. The luminal population was defined as the CD29^{Lo}CD24$^+$ population and the basal population was defined as the CD29^{Hi}CD24$^+$ population.

Whole-mount carmine staining. Whole-mount mammary fourth mammary glands were fixed in methanol Carnoy (60% methanol, 30% acetic acid, 10% chloroform) for at least 2 h and rehydrated in 70% ethanol, followed by water. Staining in carmine alum (Sigma) was done overnight and excess dye was rinsed with water. This is followed by incubation in 70%, 95%, 100% ethanol (1 h each) and fat-clearing in toluene overnight. All steps were carried out at room temperature.

Epithelial outgrowth measurement. Carmine-stained mammary glands were photographed with a Leica M80 stereomicroscope equipped with a Leica IC80 HD digital camera. The distance from the lymph node of the mammary epithelium was scored by measuring the distance between the distal edge of the lymph node and the most distal tip of the epithelium.

RNA extraction and quantitative real-time PCR. The protocol used for RNA extraction on FACS-isolated cells has been previously described[37]. Briefly, RNA extraction was performed using the RNeasy micro kit (Qiagen) according to the manufacturer's recommendations and DNase treatment. After nanodrop RNA quantification and analysis of RNA integrity, purified RNA was used to synthesize the first-strand cDNA in a 50 μl final volume, using Superscript II (Invitrogen) and random hexamers (Roche). Genomic contamination was detected by performing the same procedure without reverse transcriptase. Quantitative PCR analyses were performed with 1 ng of cDNA as template, using FastStart Essential DNA green master (Roche) and a Light Cycler 96 (Roche) for real-time PCR system.

Relative quantitative RNA was normalized using the housekeeping gene *Gapdh*. Primers were designed using PrimerBank database (http://pga.mgh.harvard.edu/primerbank/) and are listed in Supplementary Table 4. Analysis of the results was performed using Light Cycler 96 software (Roche) and relative quantification was performed using the ΔΔCt method using *Gapdh* as reference. The entire procedure was repeated in four biologically independent samples. For Extended Data Figs 6 and 7, data are shown as fold change over luminal cells or basal cells derived from 3-month-old wild-type mice (L-WT and B-WT).

Microarray analysis. Total RNA was analysed using mouse whole-genome MG-430 PM array from Affymetrix at the IRB Functional Genomics Core. All the results were normalized with RMA normalization using R-bioconductor package affy with standard parameters[38,39]. Two biologically independent samples were analysed for each condition, except for tumours derived from K5-CreER^{T2}/*Pik3ca*^{H1047R}/Rosa26-YFP or K8-CreER^{T2}/*Pik3ca*^{H1047R}/Rosa26-YFP, for which three and seven samples were analysed, respectively. Sorted BCs from K5-CreER^{T2}/Rosa26-YFP mice induced for 8 weeks or 10–12 months, LCs from K8-CreER^{T2}/Rosa26-YFP mice induced for 8 weeks or 10–12 months, BCs and LCs from K5-CreER^{T2}/*Pik3ca*^{H1047R}/Rosa26-YFP mice induced for 10–12 months, BCs and LCs from K8-CreER^{T2}/*Pik3ca*^{H1047R}/Rosa26-YFP mice induced for 8 weeks, Lin$^-$ cells from K5-CreER^{T2}/*Pik3ca*^{H1047R}/Rosa26-YFP-derived tumours and from K8-CreER^{T2}/*Pik3ca*^{H1047R}/Rosa26-YFP-derived tumours numbers 1, 2, 7, YFP$^+$ cells from K8-CreER^{T2}/*Pik3ca*^{H1047R}/Rosa26-YFP-derived tumours numbers 3, 4, 5, 6 and from K8-CreER^{T2}/*Pik3ca*^{H1047R}/*p53*$^{fl/fl}$/Rosa26-YFP-derived tumours were analysed. The gene signature induced by the expression of PIK3CA(H1047R) in each population was determined by comparing their transcriptional profile with LCs arising from age-matched K8-CreER^{T2}/Rosa26-YFP or BCs arising from K5-CreER^{T2}/Rosa26-YFP mice. Only genes upregulated or downregulated by at least 1.5 fold were considered in the analysis.

Microarray data clustering. Clustering and bootstrap analyses were performed using the pvclust and gplots packages of the R statistical suite[40]. Clustering was performed with the default parameters of the R hclust function (Euclidean distance and complete linkage) considering only the top 500 most variant genes among all experiments.

Gene signature comparison. Venn diagrams were computed with the R statistical tool. The reported hypergeometric *P* values for every comparison between two signatures correspond to the probability to observe an intersection of at least a given size by chance only, knowing the number of genes tested on a microarray chip.

Murine and human breast tumours gene expression profile comparison. To compare the murine tumour gene expression data to human tumour data, we used the METABRIC data set composed of 1,992 patients[41]. METABRIC expression data were downloaded from the EBI website (data sets EGAD00010000210 and EGAD00010000211). When multiple probes mapped to the same Entrez gene identifier, we kept the one with the highest variance in the data set using the genefu package. The PAM50 subtypes were computed using the Bioconductor genefu package dedicated function[30] (1,448 basal, 1,027 HER2$^+$, 2,260 LumB, 2,162 LumA and 323 normal).

Boxplots and Kruskal–Wallis test *P* values were computed using R. *P* values reflect the probability that at least one of the cancer subtypes express the tested signature at a significantly different level.

Uni-directional Student's *t*-test *P* values reflect the probability that one signature is significantly more expressed (or repressed) in one subtype compared to all the others. For the *t*-tests, as they are more robust to the extreme values, median and interquartile ranges were chosen as estimators of the central tendency and of the dispersion (instead of the mean and the standard deviation).

We then merged the murine data set with the METABRIC data set by keeping those genes described as orthologous in the EnsEMBL database downloaded via Biomart[42] and having exactly the same identifier. Batch effect between murine and human data was corrected using the Combat function of the Bioconductor sva package[43]. The PCA and clustering analyses were performed using the R statistical software considering an expression matrix containing only the expression values of the 46 PAM50 orthologous genes between mouse and human. For clustering, we used the Euclidean distance combined to the complete hierarchical clustering

method (default parameters). PAM50 subtypes were computed using the R/Bioconductor genefu package.

Survival analyses in humans. Mouse-derived signatures were converted to human signatures by considering the orthologous genes in humans. Signatures score were then computed and re-scaled using the dedicated function of the R/Bioconductor genefu package. The scores were computed for each patients of the METABRIC together with those present in 33 other breast tumours reference data sets[30] (7,220 patients). Survival curves were computed using the dedicated function of the genefu package only on untreated patients (1,859 cases) with available survival data. Expression level categories correspond to the tertiles of the expression values in the untreated patients. *P* values correspond to the log-rank *P* value, which reflects the probability that at least one of the class of signature expression presents a significantly differing outcome from the other classes.

31. Srinivas, S. *et al.* Cre reporter strains produced by targeted insertion of *EYFP* and *ECFP* into the *ROSA26* locus. *BMC Dev. Biol.* **1,** 4 (2001).
32. Nguyen, H., Rendl, M. & Fuchs, E. Tcf3 governs stem cell features and represses cell fate determination in skin. *Cell* **127,** 171–183 (2006).
33. Perl, A. K., Wert, S. E., Nagy, A., Lobe, C. G. & Whitsett, J. A. Early restriction of peripheral and proximal cell lineages during formation of the lung. *Proc. Natl Acad. Sci. USA* **99,** 10482–10487 (2002).
34. Jonkers, J. *et al.* Synergistic tumor suppressor activity of BRCA2 and p53 in a conditional mouse model for breast cancer. *Nature Genet.* **29,** 418–425 (2001).
35. Shehata, M., van Amerongen, R., Zeeman, A. L., Giraddi, R. R. & Stingl, J. The influence of tamoxifen on normal mouse mammary gland homeostasis. *Breast Cancer Res.* **16,** 411 (2014).
36. Rorive, S. *et al.* TIMP-4 and CD63: new prognostic biomarkers in human astrocytomas. *Mod. Pathol.* **23,** 1418–1428 (2010).
37. Beck, B. *et al.* A vascular niche and a VEGF-Nrp1 loop regulate the initiation and stemness of skin tumours. *Nature* **478,** 399–403 (2011).
38. McCall, M. N., Bolstad, B. M. & Irizarry, R. A. Frozen robust multiarray analysis (fRMA). *Biostatistics* **11,** 242–253 (2010).
39. Gentleman, R. C. *et al.* Bioconductor: open software development for computational biology and bioinformatics. *Genome Biol.* **5,** R80 (2004).
40. Suzuki, R. & Shimodaira, H. Pvclust: an R package for assessing the uncertainty in hierarchical clustering. *Bioinformatics* **22,** 1540–1542 (2006).
41. Curtis, C. *et al.* The genomic and transcriptomic architecture of 2,000 breast tumours reveals novel subgroups. *Nature* **486,** 346–352 (2012).
42. Kasprzyk, A. BioMart: driving a paradigm change in biological data management. *Database* **2011,** bar049 (2011).
43. Leek, J. T., Johnson, W. E., Parker, H. S., Jaffe, A. E. & Storey, J. D. The sva package for removing batch effects and other unwanted variation in high-throughput experiments. *Bioinformatics* **28,** 882–883 (2012).

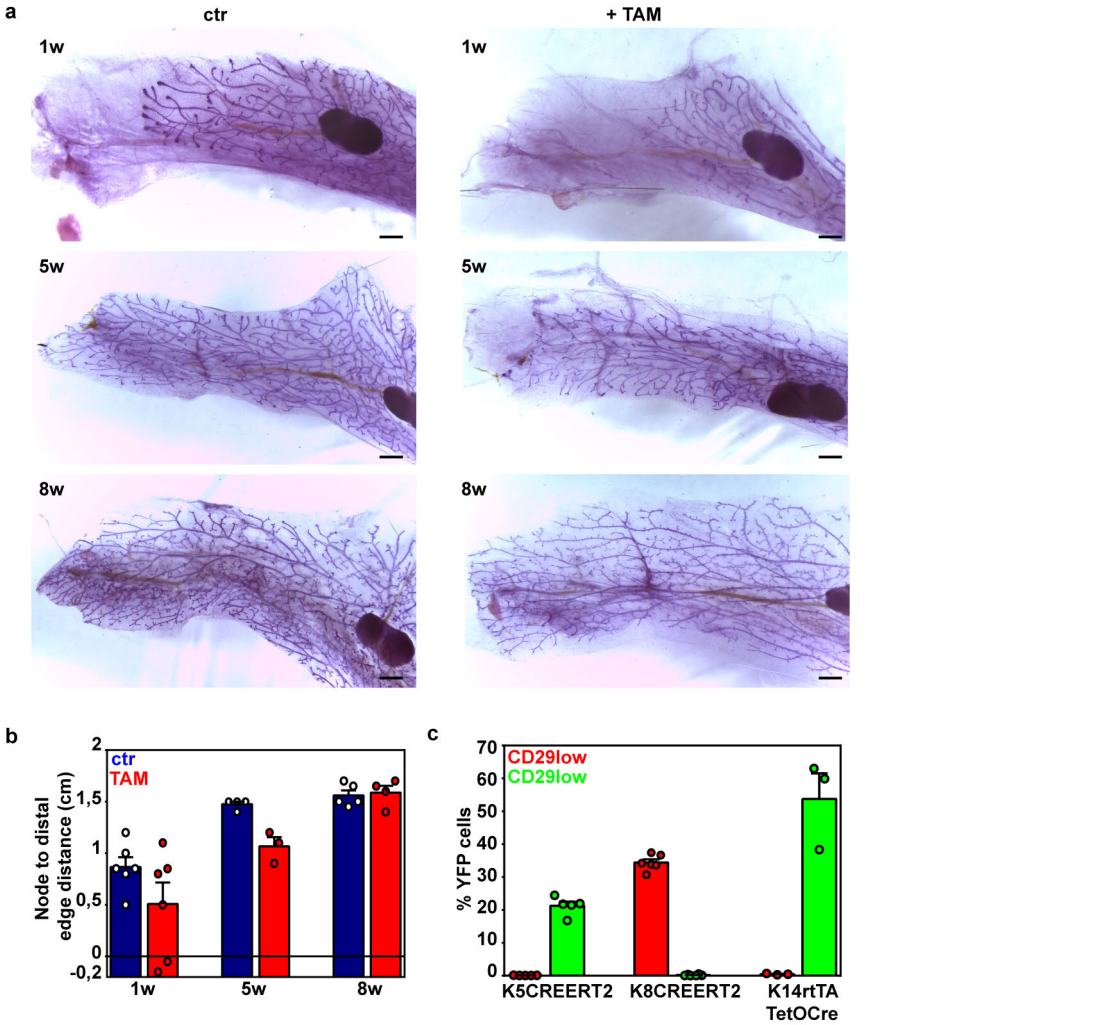

Extended Data Figure 1 | Tamoxifen administration has no long-term effect on the mammary gland. a, b, Effect of TAM on mammary epithelial postnatal growth. **a**, **b**, Representative whole-mount preparations of carmine alum-stained mammary epithelium from the fourth mammary gland, showing that TAM induces a delay in mammary epithelium growth at early time points, but no difference is observed 8 weeks after TAM induction (**a**) and mean distance from lymph node distal edge to the distal epithelial edge 1 week, 5 weeks and 8 weeks after TAM injection or oil injection (**b**) ($n = 6, 6, 4, 3, 5, 4$ mice respectively for 1 week control (ctr), 1 week TAM, 5 weeks control, 5 weeks TAM, 8 weeks control, 8 weeks TAM). *P* value derived from two-sided Student's *t*-test is 0.161, 0.035, 0.748 when comparing control and TAM conditions at 1 week, 5 weeks and 8 weeks, respectively. **c**, Percentage of YFP^+ cells in LCs ($CD29^{Lo}/CD24^+$) and in BCs ($CD29^{Hi}/CD24^+$) analysed by FACS 48 h after TAM administration in K5-$CreER^{T2}$/*Pik3ca*^{H1047R}/Rosa26-YFP and K8-$CreER^{T2}$/*Pik3ca*^{H1047R}/Rosa26-YFP, or 1 week after doxycycline administration to K14-rtTA/TetO-Cre/*Pik3ca*^{H1047R}/*p53*$^{fl/+}$/Rosa26-YFP mice ($n = 5, 6, 3$ mice respectively for K5-$CreER^{T2}$, K8-$CreER^{T2}$ and K14-rtTA/TetO-Cre). Circles, individual data points. Scale bars, 100 µm. Error bars, s.e.m.

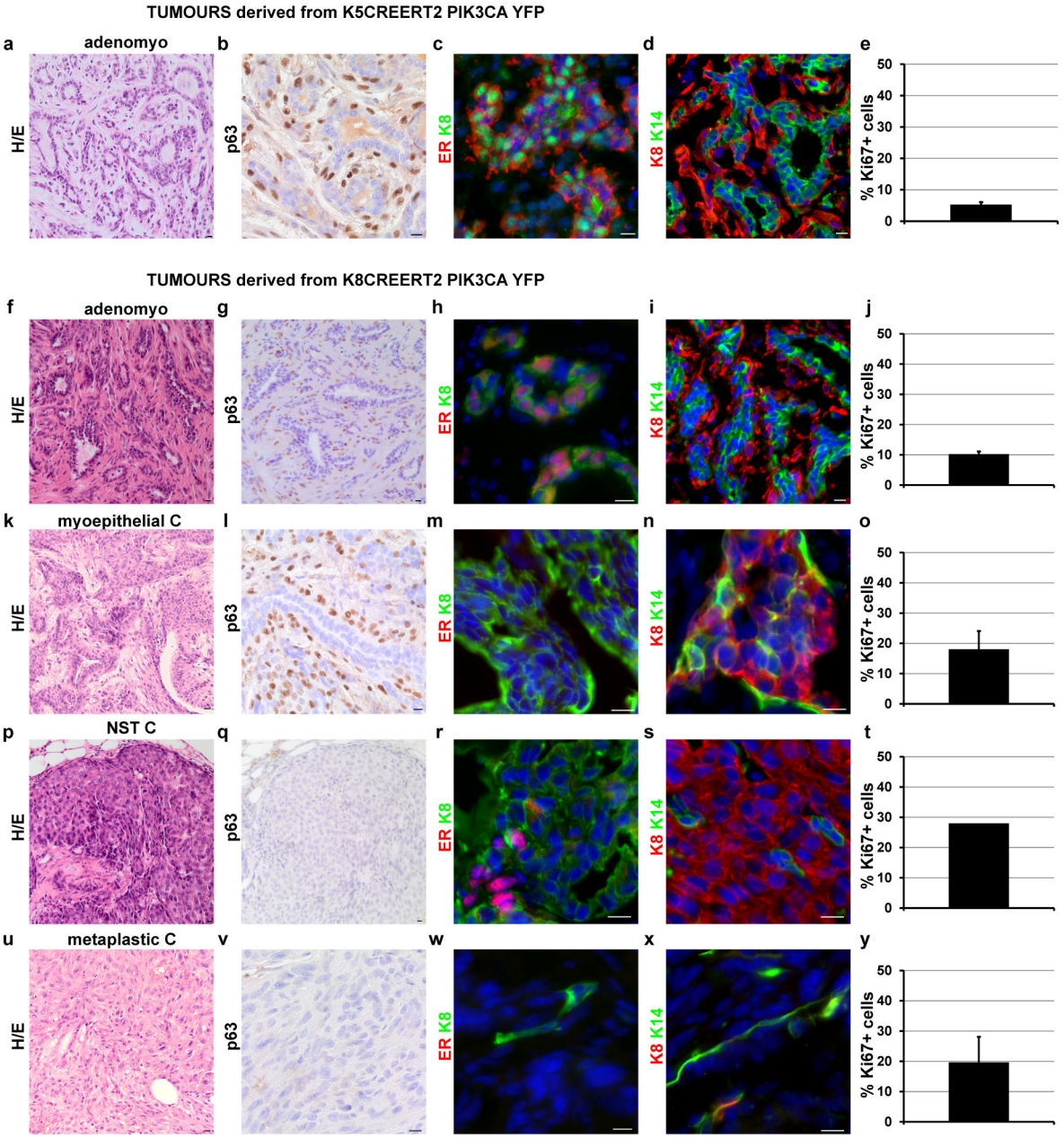

Extended Data Figure 2 | Characterization of tumours derived from basal or luminal cells upon oncogenic *Pik3ca* expression. **a**–**e**, Characterization of adenomyoepithelioma (adenomyo) tumours derived from K5-CreER^{T2}/*Pik3ca*^{H1047R}/Rosa26-YFP mice. **f**–**y**, Characterization of tumours derived from K8-CreER^{T2}/*Pik3ca*^{H1047R}/Rosa26-YFP mice. **f**–**j**, Characterization of adenomyoepithelioma. **k**–**o**, Characterization of myoepithelial carcinoma (C). **p**–**t**, Characterization of invasive carcinoma of no special type (NST C). **u**–**y**, Characterization of metaplastic carcinoma. **a**, **f**, **k**, **p**, **u**, Haematoxylin and eosin staining. **b**, **g**, **l**, **q**, **v**, p63 immunohistochemistry. **c**, **h**, **m**, **r**, **w**, Immunofluorescence of ER/K8. **d**, **i**, **n**, **s**, **x**, Immunofluorescence of K8/K14. **e**, **j**, **o**, **t**, **y**, Mean percentage of Ki67^{+} cells within tumours (n = 6, 3, 3, 1, 3 tumours and total number of cells counted = 10,408, 10,758, 11,174, 4,622, 5,732 in **e**, **j**, **o**, **t**, **y**, respectively) . Error bars, s.e.m. Scale bars, 10 μm.

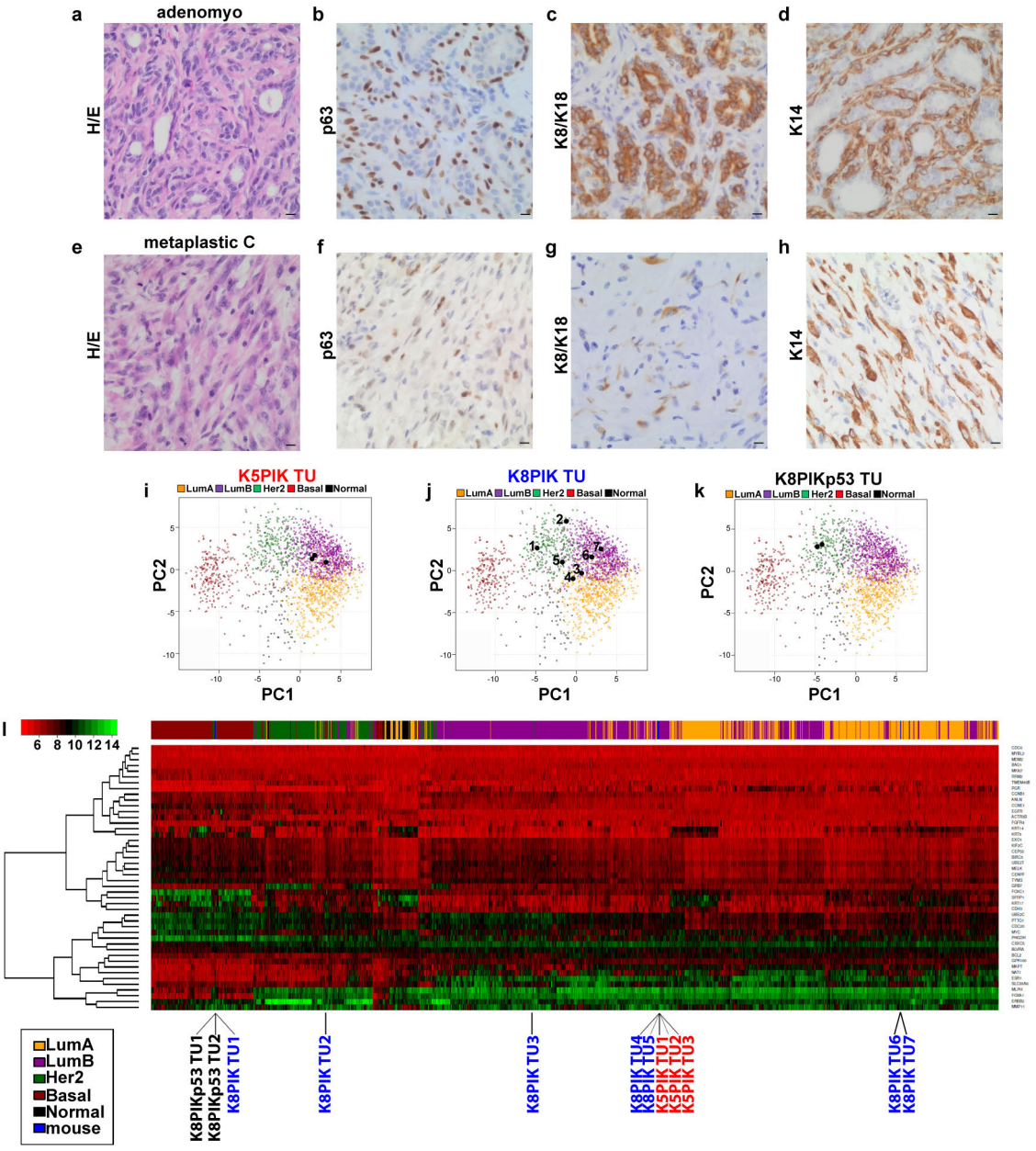

Histological classification of tumours shown

K5PIK TU1 adenomyoepithelioma
K5PIK TU2 adenomyoepithelioma
K5PIK TU3 adenomyoepithelioma
K8PIK TU1 myoepithelial carcinoma
K8PIK TU2 invasive carcinoma NST
K8PIK TU3 metaplastic carcinoma with mesenchymal differentiation
K8PIK TU4 adenomyoepithelioma
K8PIK TU5 adenomyoepithelioma
K8PIK TU6 adenomyoepithelioma+ myoepithelial carcinoma
K8PIK TU7 adenomyoepithelioma
K8PIKp53 TU1 metaplastic carcinoma with mesenchymal differentiation
K8PIKp53 TU2 metaplastic carcinoma with mesenchymal differentiation

Extended Data Figure 3 | Similarities between mouse *Pik3ca*-derived mammary tumours and human breast cancers. **a**–**d**, Human breast tumour histologically classified as adenomyoepithelioma resembling K5-CreER^{T2}/*Pik3ca*^{H1047R}/Rosa26-YFP-derived tumours (K5PIK TU). **a**, Haematoxylin and eosin staining. **b**–**d**, p63 (**b**), K8/K18 (**c**) and K14 (**d**) immunohistochemistry in the human adenomyoepithelioma. **e**–**h**, Human breast tumour histologically classified as metaplastic carcinoma resembling K8-CreER^{T2}/*Pik3ca*^{H1047R}/Rosa26-YFP derived tumours (K8PIK TU). **e**, Haematoxylin and eosin staining. **f**–**h**, p63 (**f**), K8/K18 (**g**) and K14 (**h**) immunohistochemistry in the human metaplastic carcinoma. **i**–**k**, Principal component analysis (PCA) of the METABRIC patients together with murine tumours according to the expression values of the PAM50 genes common to mice and humans. **i**, PCA of three K5-CreER^{T2}/*Pik3ca*^{H1047R} tumours (black dots) showing that these tumours cluster with human luminal B cancer subtype. **j**, PCA of seven K8-CreER^{T2}/*Pik3ca*^{H1047R}/Rosa26-YFP-derived tumours (numbered black dots). Histological classification of each numbered tumour is described below the figure. **k**, PCA of two K8-CreER^{T2}/*Pik3ca*^{H1047R}/*p53*$^{fl/fl}$/Rosa26-YFP-derived tumours (K8PIKp53 TU) (black dots) showing that these tumours cluster together with human HER2^{+} subtype. **l**, Clustering of the murine tumours among human tumours of the METABRIC data set. Clustering was performed by grouping tumours presenting similar expression patterns of PAM50 genes. Colours on top of the heatmap represent the PAM50 subtypes attributed to the human tumours. The discrepancy between PCA and clustering analysis are due to the influence of HER2 low expression in these tumours, for which around 60% of PC2 relies on ERBB2 expression. Scale bars, 10 μm.

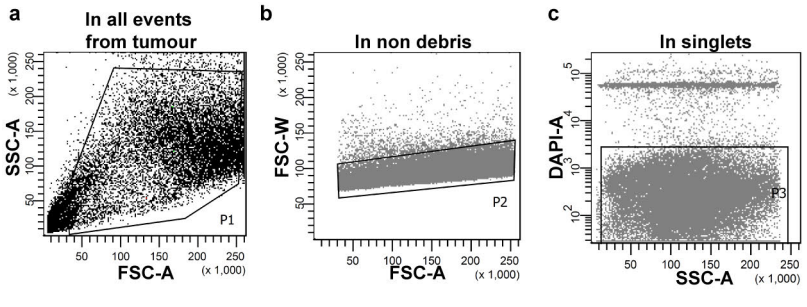

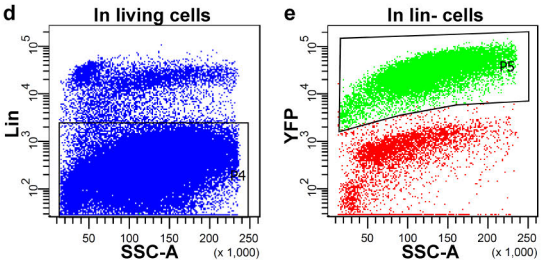

f

Population	#Events	%Parent	%Total
All Events	1,059,976	####	100.0
P1	572,614	54.0	54.0
P2	556,116	97.1	52.5
P3	516,084	92.8	48.7
P4	483,202	93.6	45.6
P5	385,036	79.7	36.3

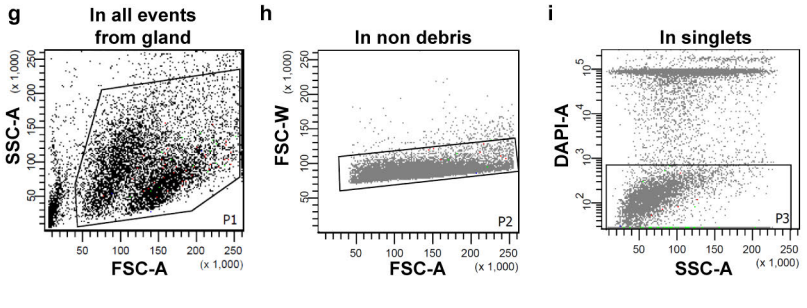

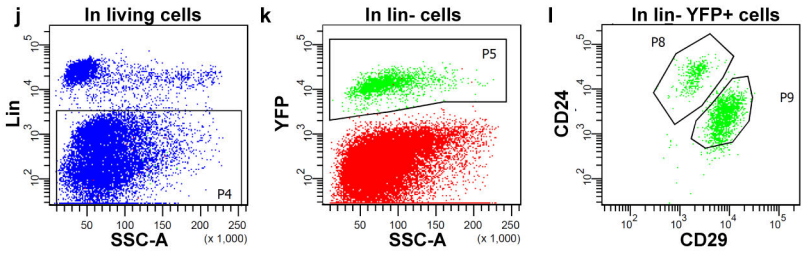

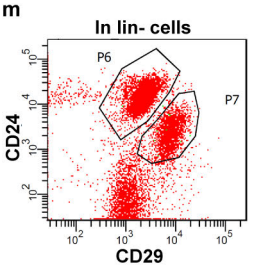

n

Population	#Events	%Parent	%Total
All Events	1,042,021	####	100.0
P1	691,158	66.3	66.3
P2	679,437	98.3	65.2
P3	360,954	53.1	34.6
P4	294,182	81.5	28.2
P5	9,230	3.1	0.9
P9	7,291	79.0	0.7
P8	1,489	16.1	0.1
P6	86,885	29.5	8.3
P7	39,644	13.5	3.8

Extended Data Figure 4 | Gating strategy to analyse and isolate tumour cells, LCs, and BCs according to their YFP, CD29 and CD24 profile. **a–e**, Dot plot FACS analysis of unicellular suspension of mammary tumour cells (in this example from K8-CreER^{T2}/*Pik3ca*-H1047R/Rosa26-YFP tumour) stained for Lin (CD31, CD45, CD140a). Debris were eliminated from all events in P1 (**a**), doublets were discarded in P2 (**b**), the living cells were gated in P3 by DAPI dye exclusion (**c**), the non-epithelial Lin$^+$ cells were discarded in P4 (**d**), and the YFP$^+$ cells were gated in P5 (**e**). **f**. Gating strategy used for FACS analysis and cell sorting, showing the proportion of parent and total cells for each gate. Tumour cells were isolated based on their Lin$^-$ profile for YFP$^-$ tumours (P4 gate), or were isolated based on their YFP profile (P5 gate) for the YFP$^+$ tumours, as described in Methods. **g–m**, Dot plot FACS analysis of unicellular suspension of mammary cells (in this example from K5-CreER^{T2}/*Pik3ca*^{H1047R}/Rosa26-YFP mice 12 months after TAM induction) stained for CD24, CD29 and Lin (CD31, CD45, CD140a). Debris were eliminated from all events in P1 (**g**), doublets were discarded in P2 (**h**), the living cells were gated in P3 by DAPI dye exclusion (**i**), the non-epithelial Lin$^+$ cells were discarded in P4 (**j**), and the YFP$^+$ cells were gated in P5 (**k**). **l**, **m**, CD29 and CD24 expression were used to gate the CD29^{Lo}CD24$^+$ population, corresponding to LCs, and to gate the CD29^{Hi}CD24$^+$ population, corresponding to BCs, either in YFP$^+$ cells (**l**) or in Lin$^-$ cells (**m**). **n**, Gating tree showing the gating strategy used for FACS analysis and sorting, showing the proportion of parent and total cells for each gate.

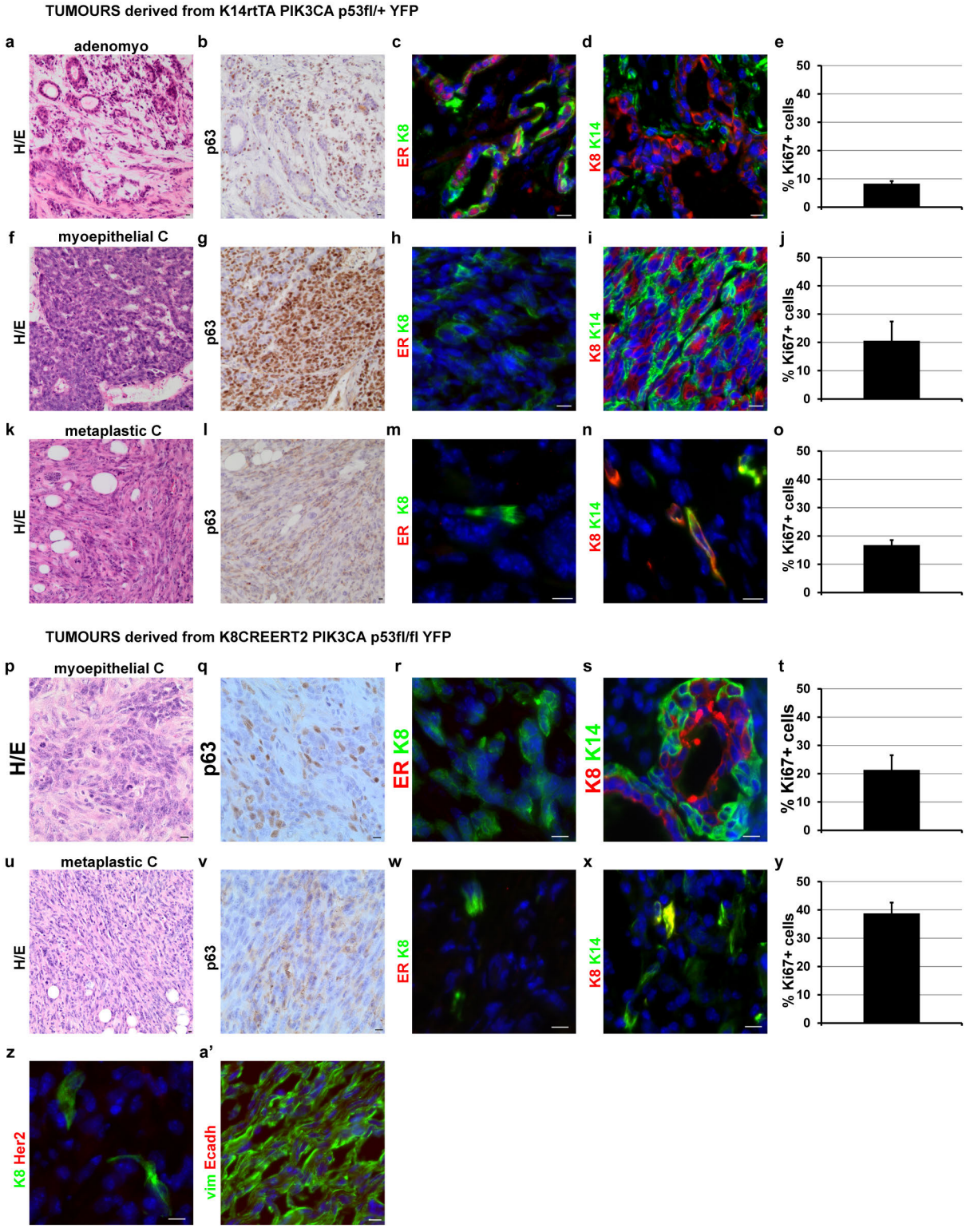

Extended Data Figure 5 | Characterization of tumours derived from BCs or LCs upon concomitant expression of oncogenic *Pik3ca* and deletion of *p53*. **a**–**o**, Characterization of tumours derived from K14-rtTA/TetO-Cre/*Pik3ca*^{H1047R}/*p53*$^{fl/+}$/Rosa26-YFP mice. **a**–**e**, Characterization of adenomyo-epithelioma (adenomyo). **f**–**j**, Characterization of myoepithelial carcinoma. **k**–**o**, Characterization of metaplastic carcinoma. **p**–**a′**, Characterization of tumours derived from K8-CreER^{T2}/*Pik3ca*^{H1047R}/*p53*$^{fl/fl}$/Rosa26-YFP mice. **p**–**t**, Characterization of myoepithelial carcinoma (C). **u**– **a′**, Characterization of metaplastic carcinoma. **a**, **f**, **k**, **p**, **u**, Haematoxylin and eosin staining. **b**, **g**, **l**, **q**, **v**, p63 immunohistochemistry. **c**, **h**, **m**, **r**, **w**, Immunofluorescence of K8/ER. **d**, **i**, **n**, **s**, **x**, Immunofluorescence of K8/K14. **e**, **j**, **o**, **t**, **y**, Mean percentage of Ki67^{+} cells within tumours (n = 4, 3, 3, 4, 6 tumours and total cells counted = 11,903, 10,670, 6,992, 14,743, 8,172 in **e**, **j**, **o**, **t**, **y**, respectively). **z**, Immunofluorescence of K8/HER2. **a′**, Immunofluorescence of E-cadherin/vimentin. Error bars, s.e.m. Scale bars, 10 µm.

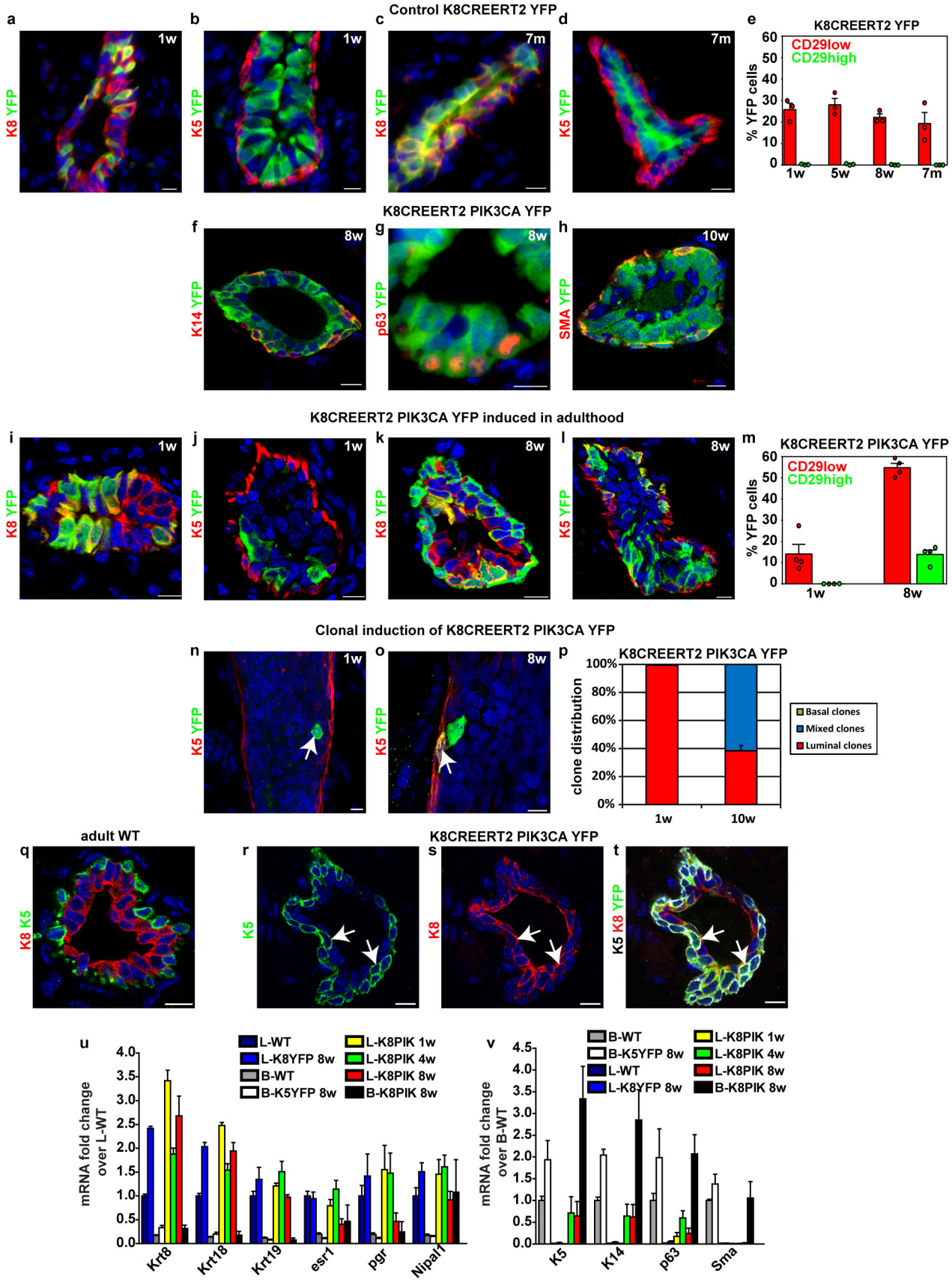
Control K8CREERT2 YFP
K8CREERT2 YFP
CD29low
CD29high
% YFP cells
K8CREERT2 PIK3CA YFP
K8CREERT2 PIK3CA YFP induced in adulthood
Clonal induction of K8CREERT2 PIK3CA YFP
clone distribution
Basal clones
Mixed clones
Luminal clones
adult WT
mRNA fold change over L-WT
L-WT
L-K8YFP 8w
B-WT
B-K5YFP 8w
L-K8PIK 1w
L-K8PIK 4w
L-K8PIK 8w
B-K8PIK 8w
Krt8
Krt18
Krt19
esr1
pgr
Nipal1
mRNA fold change over B-WT
K5
K14
p63
Sma

Extended Data Figure 6 | Oncogenic *Pik3ca* expression induces multipotency in unipotent luminal progenitors. **a**–**d**, Immunofluorescence showing the expression of K8/YFP (**a**, **c**) or K5/YFP (**b**, **d**) 1 week (**a**, **b**) and 7 months (**c**, **d**) after TAM injection in control K8-CreER^{T2}/Rosa26-YFP mammary gland. **e**, Percentage of YFP^{+} cells in LCs (CD29^{Lo}/CD24^{+}) and in BCs (CD29^{Hi}/CD24^{+}) at different time points after TAM administration to K8-CreER^{T2}/Rosa26-YFP mice ($n = 3$ mice per time point) showing that no YFP^{+} cells expressing CD29^{Hi}/CD24^{+} were detected in control K8-CreER^{T2}/Rosa26-YFP mammary glands at any time point. **f**–**h**. Immunofluorescence of K14/YFP (**f**), p63/YFP (**g**), SMA/YFP (**h**) 8 weeks (**f**, **g**) or 10 weeks (**h**) after TAM administration to K8-CreER^{T2}/*Pik3ca*^{H1047}/Rosa26-YFP mice, shows that the BCs arising from LCs upon oncogenic *Pik3ca* targeting expressed these classical markers of BCs. **i**–**m**, Induction of *Pik3ca*^{H1047R} expression in LCs in adult mice. **i**–**l**, Immunofluorescence showing the expression of K8/YFP (**i**, **k**) or K5/YFP (**j**, **l**) 1 week (**i**, **j**) and 8 weeks (**k**, **l**) after TAM injection in K8-CreER^{T2}/*Pik3ca*^{H1047R}/Rosa26-YFP mice induced in adulthood. **m**, Percentage of YFP^{+} cells in LCs (CD29^{Lo}/CD24^{+}) and in BCs (CD29^{Hi}/CD24^{+}) at different time points after TAM administration to K8-CreER^{T2}/*Pik3ca*^{H1047R}/Rosa26-YFP mice induced in adulthood ($n = 4$ mice per time point). **n**, **o**, Immunofluorescence of K5/YFP showing the clonal YFP expression in a single isolated LC 1 week after TAM injection (**n**), and 8 weeks after TAM injection showing a clone that gave rise to an LC and a BC (**o**) in K8-CreER^{T2}/*Pik3ca*^{H1047R}/Rosa26-YFP mammary gland. Arrow in **n** points to the isolated LC, while arrow in **o** points to the newly arisen BC. **p**, Distribution of clones 1 week or 10 weeks after TAM injection in K8-CreER^{T2}/*Pik3ca*^{H1047R}/Rosa26-YFP at clonal dose. Clones were scored as composed of only luminal cells (luminal clones), composed of only basal cells (basal clones) or composed of luminal and basal cells (mixed clones) ($n = 4$ mice per time point). See Methods for more details. **q**–**t**, Immunofluorescence of K5/K8 (**q**), K5 (**r**), K8 (**s**) and K5/K8/YFP (**t**) shows that in wild-type mammary gland, K5 and K8 are not co-expressed (**q**), while K5/K8 double-positive cells are observed in K8-CreER^{T2}/*Pik3ca*^{H1047R}/Rosa26-YFP mammary gland 8 weeks after oncogenic *Pik3ca* expression in LCs (**r**–**t**). Arrows in **r**–**t** point to K5^{+}K8^{+}YFP^{+} cells. **u**, **v**, RT–PCR analysis of luminal (**u**) or basal (**v**) genes in YFP^{+} LCs and BCs sorted from K8-CreER^{T2}/*Pik3ca*^{H1047R}/Rosa26-YFP mice induced for 1 week, 4 weeks or 8 weeks, in YFP^{+} LCs derived from K8-CreER^{T2}/Rosa26-YFP and in YFP^{+} BCs derived from K5-CreER^{T2}/Rosa26-YFP mice induced for 8 weeks. Data for luminal genes are compared to adult wild-type LCs (**u**) while data for basal genes are compared to adult wild-type BCs (**v**) ($n = 4$ biologically independent samples per condition). Circles, individual data points. Scale bars, 10 μm. Error bars, s.e.m.

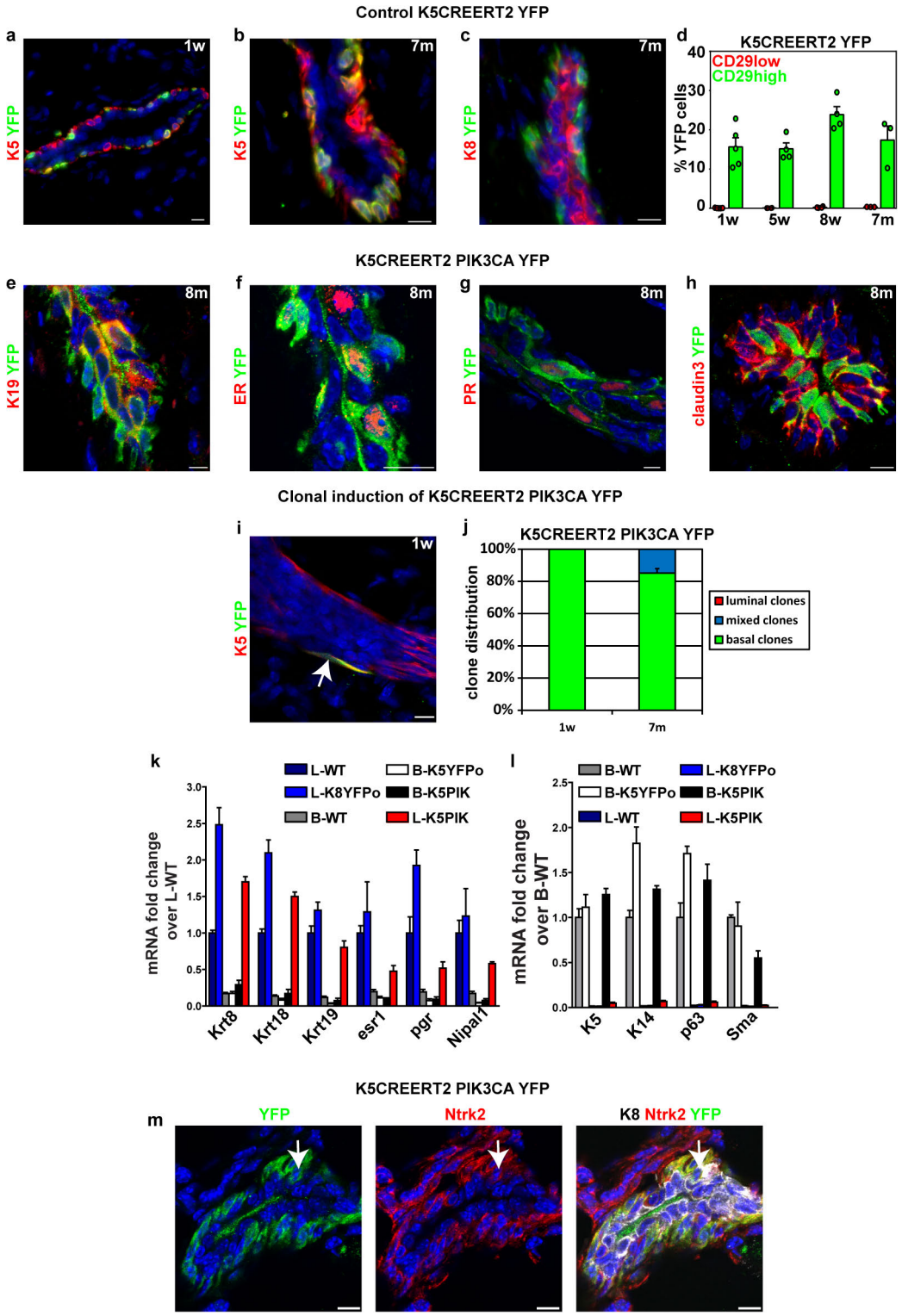
Control K5CREERT2 YFP
a
1w
K5 YFP
b
7m
K5 YFP
c
7m
K8 YFP
d
K5CREERT2 YFP
CD29low
CD29high
% YFP cells
40
30
20
10
0
1w
5w
8w
7m
K5CREERT2 PIK3CA YFP
e
8m
K19 YFP
f
8m
ER YFP
g
8m
PR YFP
h
8m
claudin3 YFP
Clonal induction of K5CREERT2 PIK3CA YFP
i
1w
K5 YFP
j
K5CREERT2 PIK3CA YFP
100%
80%
60%
40%
20%
0%
clone distribution
1w
7m
luminal clones
mixed clones
basal clones
k
L-WT
B-K5YFPo
L-K8YFPo
B-K5PIK
B-WT
L-K5PIK
mRNA fold change over L-WT
3.0
2.5
2.0
1.5
1.0
0.5
0.0
Krt8
Krt18
Krt19
esr1
pgr
Nipal1
l
B-WT
L-K8YFPo
B-K5YFPo
B-K5PIK
L-WT
L-K5PIK
mRNA fold change over B-WT
2.5
2.0
1.5
1.0
0.5
0.0
K5
K14
p63
Sma
K5CREERT2 PIK3CA YFP
m
YFP
Ntrk2
K8 Ntrk2 YFP

Extended Data Figure 7 | Oncogenic *Pik3ca* expression induces multipotency in unipotent basal progenitors. **a**–**c**, Immunofluorescence showing the expression of K5/YFP (**a**, **b**) or K8/YFP (**c**) at 1 week (**a**) and 7 months (**b**, **c**) in control K5-CreER^{T2}/Rosa26-YFP mammary gland. **d**, Percentage of YFP^{+} cells in LCs (CD29^{Lo}/CD24^{+}) and in BCs (CD29^{Hi}/CD24^{+}) at different time points after TAM administration to K5-CreER^{T2}/Rosa26-YFP ($n = 5, 4, 4, 3$ mice for 1 week, 8 weeks, 7 months and 12 months, respectively) showing that no YFP^{+} cells expressing CD29^{Lo}/CD24^{+} were detected in control K5-CreER^{T2}/Rosa26-YFP mammary glands at any time point. **e**–**h**, Immunofluorescence of K19/YFP (**e**), ER/YFP (**f**), PR/YFP (**g**), claudin 3/YFP (**h**), 8 months after TAM administration to K5-CreER^{T2}/*Pik3ca*^{H1047}/Rosa26-YFP mice, shows that LCs arising from BCs upon oncogenic *Pik3ca* targeting expressed these classical markers of LCs. **i**, Immunofluorescence of K5/YFP showing the YFP expression in a single isolated BC 1 week after TAM injection at a clonal dose. Arrow points to the isolated BC. **j**, Distribution of clones 1 week or 7 months after TAM injection in K5-CreER^{T2}/*Pik3ca*^{H1047R}/Rosa26-YFP at a clonal dose. Clones were scored as composed of only luminal cells (luminal clones), composed of only basal cells (basal clones) or composed of luminal and basal cells (mixed clones) ($n = 3, 4$ mice for 1 week and 7 months, respectively). See Methods for more details. **k**, **l**, RT–PCR analysis of luminal (**k**) or basal (**l**) genes in YFP^{+} LCs and BCs sorted from K5-CreER^{T2}/*Pik3ca*^{H1047R}/Rosa26-YFP mice induced for 10–12 months, in YFP^{+} LCs derived from K8-CreER^{T2}/Rosa26-YFP mice and in YFP^{+} BCs derived from K5-CreER^{T2}/Rosa26-YFP mice induced for 10–12 months. Data for luminal genes are compared to adult wild-type LCs (**k**) while data for basal genes are compared to adult wild-type BCs (**l**) ($n = 4$ biologically independent samples per condition). **m**, Confocal microscopy analysis of immunofluorescence of YFP, TrkB and K8 of mammary glands 7 months after *Pik3ca* expression in BCs, showing that the newly formed LCs after Pik3ca expression in BCs co-expressed Nrtk2 and K8. Arrow points to formed K8^{+}/Nrtk2^{+}/YFP^{+} cell. Circles, individual data points. Scale bars, 10 μm. Error bars, s.e.m.

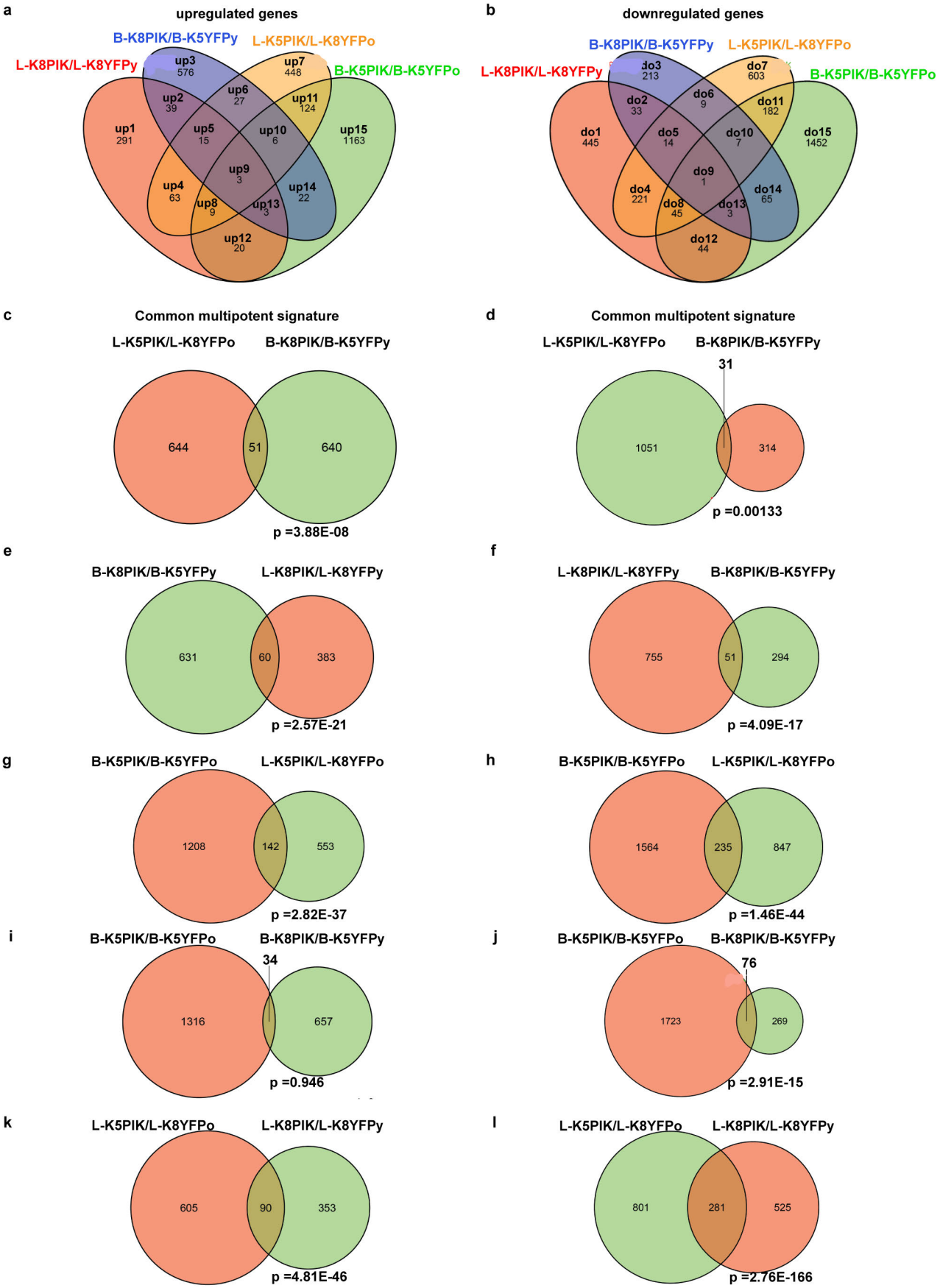
a
upregulated genes
B-K8PIK/B-K5YFPy
L-K5PIK/L-K8YFPo
L-K8PIK/L-K8YFPy
B-K5PIK/B-K5YFPo
up1 291
up2 39
up3 576
up4 63
up5 15
up6 27
up7 448
up8 9
up9 3
up10 6
up11 124
up12 20
up13 3
up14 22
up15 1163
b
downregulated genes
B-K8PIK/B-K5YFPy
L-K5PIK/L-K8YFPo
L-K8PIK/L-K8YFPy
B-K5PIK/B-K5YFPo
do1 445
do2 33
do3 213
do4 221
do5 14
do6 9
do7 603
do8 45
do9 1
do10 7
do11 182
do12 44
do13 3
do14 65
do15 1452
c
Common multipotent signature
L-K5PIK/L-K8YFPo
B-K8PIK/B-K5YFPy
644
51
640
p =3.88E-08
d
Common multipotent signature
L-K5PIK/L-K8YFPo
B-K8PIK/B-K5YFPy
31
1051
314
p =0.00133
e
B-K8PIK/B-K5YFPy
L-K8PIK/L-K8YFPy
631
60
383
p =2.57E-21
f
L-K8PIK/L-K8YFPy
B-K8PIK/B-K5YFPy
755
51
294
p =4.09E-17
g
B-K5PIK/B-K5YFPo
L-K5PIK/L-K8YFPo
1208
142
553
p =2.82E-37
h
B-K5PIK/B-K5YFPo
L-K5PIK/L-K8YFPo
1564
235
847
p =1.46E-44
i
B-K5PIK/B-K5YFPo
B-K8PIK/B-K5YFPy
34
1316
657
p =0.946
j
B-K5PIK/B-K5YFPo
B-K8PIK/B-K5YFPy
76
1723
269
p =2.91E-15
k
L-K5PIK/L-K8YFPo
L-K8PIK/L-K8YFPy
605
90
353
p =4.81E-46
l
L-K5PIK/L-K8YFPo
L-K8PIK/L-K8YFPy
801
281
525
p =2.76E-166

Extended Data Figure 8 | Molecular characterization of oncogenic *Pik3ca* induced multipotency. **a**, **b**, Venn diagram representing the common and distinct upregulated (**a**) and downregulated (**b**) genes in BCs and LCs after *Pik3ca* expression in BCs and LCs compared to age-matched control BCs and LCs, respectively, with the name of the list of genes and number of genes in each section. The list of genes in each Venn section is provided in Supplementary Tables 2 and 3. **c**–**l**, Venn diagrams representing the common genes upregulated (**c**, **e**, **g**, **i**, **k**) or downregulated (**d**, **f**, **h**, **j**, **l**) in the newly generated LCs or BCs after $Pik3ca^{H1047R}$ expression in unipotent progenitors (**c**, **d**); in LCs and in BCs after $Pik3ca^{H1047R}$ expression in LCs (genes regulated following the initial targeting of $Pik3ca^{H1047R}$ in LCs, and thus reflecting the LC of origin) (**e**, **f**); in LCs and in BCs after $Pik3ca^{H1047R}$ expression in BCs (genes regulated by $Pik3ca^{H1047R}$ in BCs, and thus reflecting the BC of origin) (**g**, **h**); in BCs after $Pik3ca^{H1047R}$ expression in LCs and in BCs (genes regulated by $Pik3ca^{H1047R}$ expression in BCs, irrespective of cell of origin) (**i**, **j**); in LCs after $Pik3ca^{H1047R}$ expression in BCs and in LCs (genes regulated by $Pik3ca^{H1047R}$ expression in LCs, irrespective of cell of origin) (**k**, **l**). Diameter of the diagram is proportional to the number of genes it contains. The reported hypergeometric *P* values correspond to the probability of observing an intersection of this size by chance only, knowing the number of genes tested on a microarray chip.

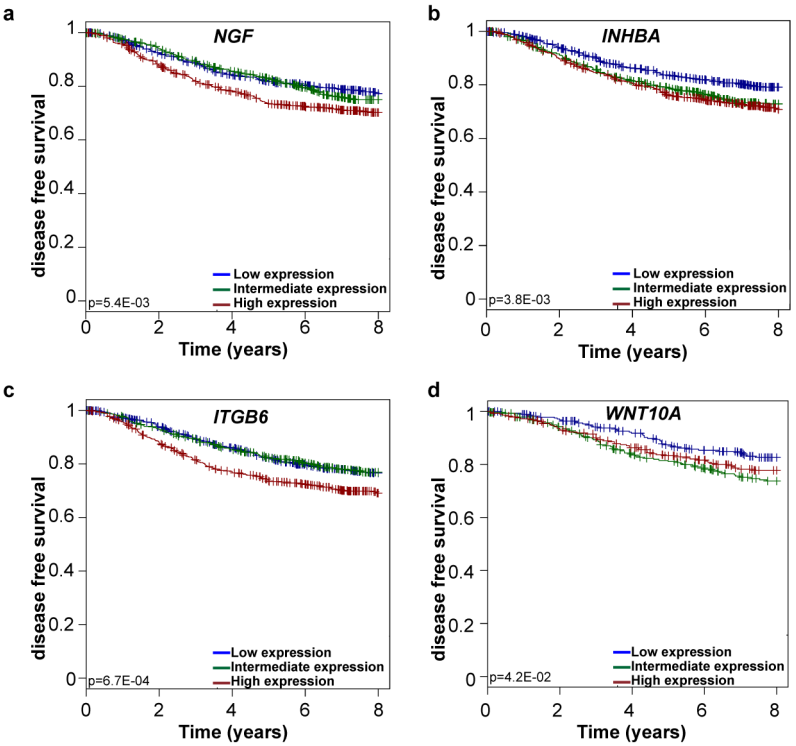

Extended Data Figure 9 | Genes of luminal-to-basal multipotency signature correlate with patient outcome in untreated breast cancer patients. a–d, Disease-free survival in untreated patients according to the level of expression (low = blue, intermediate = green or high = red) of the genes in the luminal-to-basal multipotency signature, namely *NGF* (**a**), *INHBA* (**b**), *ITGB6* (**c**) and *WNT10A* (**d**), showing that genes of luminal-to-basal multipotency signature predict disease-free survival in untreated breast cancer patients. Patients expressing high levels of this signature are more prone to tumour relapse while those expressing lower levels of this signature show lower rates of relapse. The log-rank *P* values account for the significance of this difference.

Author Queries

Journal: **Nature**
Paper: **nature14665**
Title: **Reactivation of multipotency by oncogenic PIK3CA induces breast tumour heterogeneity**

Query Reference	Query
1	AUTHOR: A PDF proof will be produced on the basis of your corrections to this preproof and will contain the main-text figures edited by us and the Extended Data items supplied by you (which may have been resized but will not have been edited otherwise by us).
2	When you receive the PDF proof, please check that the display items are as follows (doi:10.1038/nature14665): Figs 3p, 4g, i (black & white); 1a–f, 2a–i, 3a–o, 4a–f, h, j–l (colour); Tables: None; Boxes: None; Extended Data display items: Figs 1–9.
3	Please check the edits to all main-text figures (and tables, if any) very carefully, and ensure that any error bars in the figures are defined in the figure legends. If you wish to revise the Extended Data items for consistency with main-text figures and tables, please copy the style shown in the PDF proof (such as italicising variables and gene symbols, and using initial capitals for labels) and return the revised Extended Data items to us along with your proof corrections.
4	Author: We assume no power analysis was done to estimate sample size; per our reporting guidelines we will include the statement 'No statistical methods were used to predetermine sample size.' Please edit if appropriate.
5	Author: We assume there was no randomization; per our reporting guidelines, we will include the statement ''The experiments were not randomized''. Also, we assume that there was no blinding; per our reporting guidelines, we will include the statement ''The investigators were not blinded to allocation during experiments and outcome assessment''. Please edit either of these statements if necessary.
6	Author: OK?
7	Author: OK?
Web summary	PIK3CA mutations are associated with distinct types of human breast cancers but the cellular origin and mechanisms responsible for this heterogeneity were unclear; here, using a genetic approach in mice, PIK3CA mutations are shown to activate a genetic program directing multiple cell fates in normally lineage-restricted cell types.

For Nature office use only:

Layout	☐	Figures/Tables/Boxes	☐	References	☐
DOI	☐	Error bars	☐	Supp info	☐
Title	☐	Colour	☐	Acknowledgements	☐
Authors	☐	Text	☐	Author contribs	☐
Addresses	☐	Methods	☐	COI	☐
First para	☐	Received/Accepted	☐	Correspondence	☐
		AOP	☐	Author corrx	☐
		Extended Data	☐	Web summary	☐
				Accession codes link	☐